Finite element approximation of electromagnetic fields using non-fitting meshes for Geophysics

Théophile Chaumont-Frelet, Serge Nicaise, David Pardo

FINITE ELEMENT APPROXIMATION OF ELECTROMAGNETIC FIELDS USING NON-FITTING MESHES FOR GEOPHYSICS

THÉOPHILE CHAUMONT-FRELET, SERGE NICAISE, AND DAVID PARDO

Abstract. We analyze the use of non-fitting meshes for simulating the propagation of electromagnetic waves inside the Earth. In order to take into account subcell conductivity variations, we propose a simple "exact integration technique" that avoids the use of parameter homogenization and employs standard edge finite element basis functions. For our geophysical applications, we consider a 3D Maxwell's system with piecewise constant conductivity and globally constant permittivity and permeability. The model is analysed and discretized using both the E and H-formulations. Our main contribution is to develop a sharp error estimate for both the electric and magnetic fields. In the presence of singularities, our estimate shows that the magnetic field approximation is converging faster than the electric field approximation. As a result, we conclude that error estimates available in the literature for Nédélec's elements with fitting meshes are sharp with respect to the electric field error, but provide pessimistic convergence rates for the magnetic field in our geophysical applications. Another surprising consequence of our analysis is that non-fitting meshes deliver the same convergence rate than fitting meshes to approximate the magnetic field. Our theoretical results are numerically illustrated *via* 2D experiments. For the analyzed cases, the accuracy loss due to the use of non-fitting meshes is limited, even for high conductivity contrasts.

Introduction

Electromagnetic (EM) methods are used in Geophysics for reservoir characterization, and more generally, subsurface imaging. EM methods are sensitive to the high conductivity contrast that occurs between oil-saturated and water-saturated rocks. For this reason, they are routinely employed in geophysical surveys, such as well logging [17] (including laterolog [32], logging-while-drilling [31], through casing [33] and cross-well configurations [37]), controlled source EM [14], and magnetotellurics [36].

Forward modelling of the electromagnetic fields is a key aspect of the aforementioned applications. It is either used directly to compare a synthetic model to *in-situ* measurements, or as part of an inversion algorithm if the aim is to reconstruct a conductivity model from observed data [20]. In both cases, it is crucial to design a forward modelling method that is fast, accurate, and robust [3].

To describe the propagation of electromagnetic fields inside the Earth, we consider 3D Maxwell's equations in a convex isotropic domain. The permittivity and permeability are assumed to be constant and the conductivity is taken piecewise constant onto a polyhedral partition of the domain. Apart from the isotropy assumption, these hypothesis are rather general regarding geophysical applications.

Different discretization techniques are available to solve 3D Maxwell's equations [3]. Here, we restrict to first order edge finite element (FE) discretizations (also known as Nédélec's elements [29]) and consider both electric and magnetic field formulations.

In FE methods, the mesh is typically aligned with the conductivity model. However, this mesh design constraint presents important limitations. On the other hand, non-fitting meshes permit to simplify implementations and/or reduce computational costs. Figure 1 depicts a well logging application. As shown there, non-fitting meshes allow the user to design a single "sliding" mesh adapted to the tool configuration (sources, receivers and skin-depth) and to use it for different tool positions. Other interesting applications include layers or shapes that are smaller than the mesh cell size, or taking into account inclined layers into a cartesian grid mesh, as in [28]. More generally, in the context of inverse problems, non-fitting meshes enable the user to employ the same mesh for all iterations, and to decouple the discretization of the forward problem with the conductivity model representation [20].

Here, we focus on the use of "non-fitting" meshes, where the conductivity may be discontinuous on the interior of an element. Standard Lagrange and Nédélec's elements are known to perform well only if the medium parameters are smooth inside each mesh cell. In presence of non-fitting meshes, a usual technique is then to use homogenization or averaging formulae to upscale a varying parameter to one constant value inside each cell.

In the simplest case, the averaging consists of an explicit formula [24, 28, 21]. However, these averaging formulae are rigorously validated only under some specific assumptions, such as small-scale periodicity or one-dimensional variations. In order to overcome these difficulties, "numerical homogenization" techniques have been developed. The homogenized parameter can be obtained through the solution of a local problem inside each cell [18]. In general, numerical homogenization can be linked to multiscale methods, and the parameter upscaling algorithm can be viewed as a particular choice of basis functions satisfying a local boundary value problem [22, 34, 4].

In the context of seismic wave propagation problems, similar averaging techniques are currently used [5, 10]. Recently, a simpler technique, which avoids the use of averaging, homogenization and multiscale basis functions has been introduced by T. Chaumont-Frelet and collaborators for the propagation of acoustic waves inside the Earth [7, 11]. The main idea is to keep unmodified the basis functions and the Earth model. Subcell variations of the model are then taken into account through accurate quadrature schemes. We will refer to this technique as the "exact quadrature technique", since the essence of the method is just to use standard finite element shape functions, and exactly (or at least, sufficiently accurately) integrate the corresponding variational formulation. In the context of seismic wave propagation, the exact quadrature technique is proven to be numerically efficient [6] and a convergence analysis shows that the method is well-suited to approximate high-frequency waves, even if the solution can be rough inside the mesh cells [12]. The method is also compared to an averaging technique in [11], where it is shown that the exact integration technique outperforms averaging, especially when the characteristic size of the heterogeneities is not small enough compared to the solution wavelength.

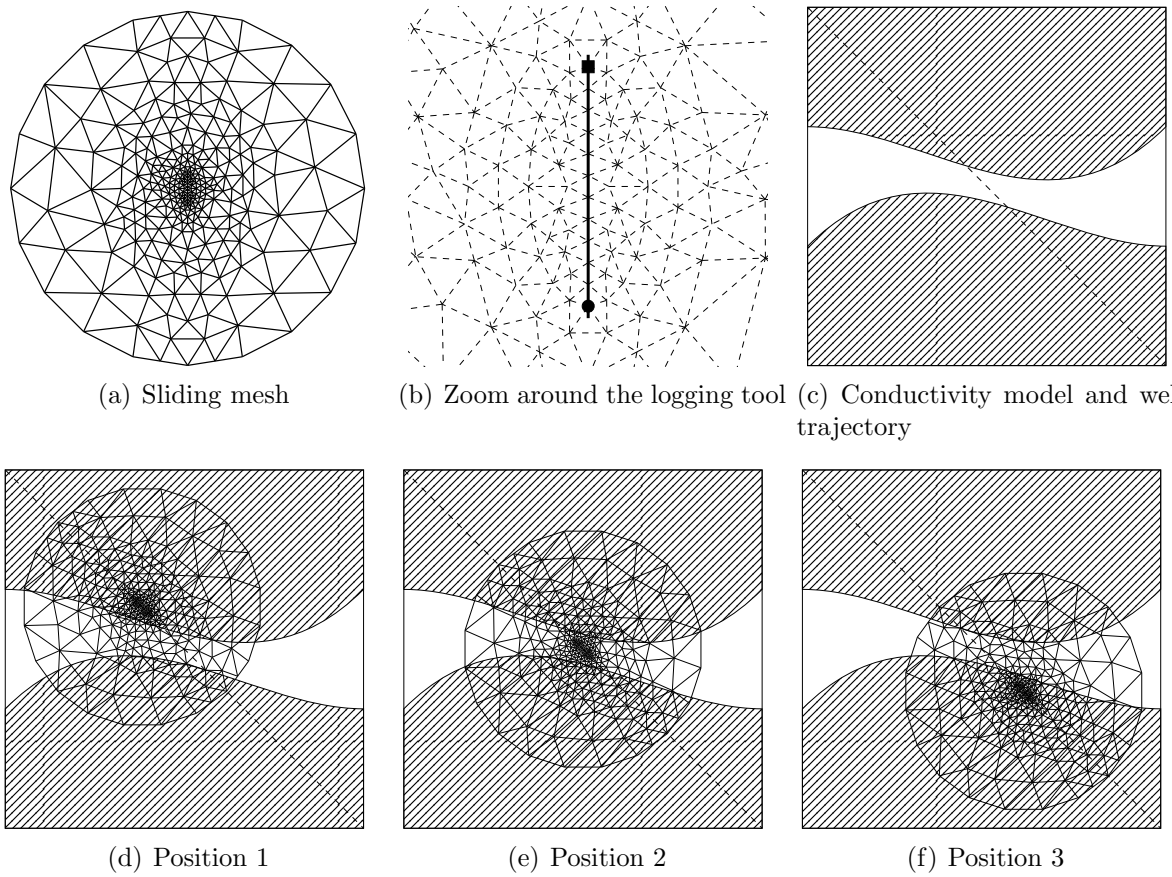

(a) Sliding mesh (b) Zoom around the logging tool (c) Conductivity model and well trajectory

(d) Position 1 (e) Position 2 (f) Position 3

FIGURE 1. Sliding mesh

The key point in the success of the exact quadrature technique for wave propagation is that most of the error is due to dispersion [12]. When considering Maxwell's system for Geophysics, the situation is different, because the Earth highly absorbs electromagnetic waves, so that dispersion errors are small. As a result, the main advantages and limitations of an exact quadrature technique for EM problems are unclear.

In this work, we investigate the possible advantages of using the exact quadrature technique for EM geophysical applications. To do so, we develop a rigorous convergence analysis of the aforementioned finite element methods. Though our aim is to investigate non-fitting mesh discretizations, it turns out that our main result is also useful for fitting meshes. Since we focus on geophysical applications, the medium permeability is constant and the magnetic field always exhibits H^1 regularity. On the other hand, because the conductivity is piecewise constant, the electric field only presents H^s regularity, where $0 < s \leq 1$ can be arbitrary small, depending on the conductivity contrasts [15].

Recent $H(curl)$-norm error estimates exist in the literature [23, 27]. These results are optimal in the $H(curl)$-norm and predict a $\mathcal{O}(h^s)$ convergence rate in this configuration. The $H(curl)$-norm can be viewed as a weighted sum of the L^2-norms of the electric and

magnetic fields. Therefore, the aforementioned estimate predicts at least convergence rates of $\mathcal{O}(h^s)$ for both the electric and magnetic fields in the L^2-norm.

Here, we focus on proving optimal L^2 error estimates for both the electric and magnetic fields. We classically demonstrate that the electric field approximation converges as $\mathcal{O}(h^s)$. The novel result is that the magnetic field error decreases as $\mathcal{O}(h^{\min(1,2s)})$, its proof relies on a sort of Aubin-Nitsche's trick.

An interesting consequence is that both fitting and non-fitting meshes deliver the same convergence rate for the magnetic field. In order to illustrate this feature, let us consider a layered medium without singularities. In this case [15], the electric field exhibits local H^1 regularity inside each layer, but only $H^{(1-\delta)/2}$ global regularity ($\delta > 0$ being an arbitrarily small, but strictly positive constant), since the normal component jumps across each interface. Because both fields are locally H^1, standard convergence arguments indicate linear convergence rates for both electromagnetic fields if a fitting mesh is used. If a non-fitting mesh is used, then the electric field only converges as $\mathcal{O}(h^{(1-\delta)/2})$. However, our new estimate shows that the magnetic field error decreases as $\mathcal{O}(h^{1-\delta})$, that is, the convergence rate of the magnetic field approximation is almost linear, even for non-fitting meshes. This observation actually extends to general conductivity models with singularities. Hence, an important conclusion of our work is that fitting and non-fitting meshes virtually provide the same convergence rate for the magnetic field approximation.

Our convergence theory is validated and illustrated using 2D numerical experiments. We consider the H-formulation and the E-formulation in layered media for the TE and TM-polarizations, respectively. In these test cases, we carefully compare the accuracy between fitting and non-fitting meshes as well as the impact of the conductivity contrast on the precision. We also analyse an experiment with crossing interfaces generating a singular solution for the TM-polarization. These numerical tests show that our convergence analysis is sharp, and that fitting and non-fitting meshes virtually provide the same accuracy for the magnetic field approximation.

The proofs we provide are carried out for the 3D Maxwell's system, and the techniques we use are typical of finite element analysis. The main conclusion stating that increased accuracy can be expected for the magnetic field shall be useful in analysing other discretization techniques like finite differences [3], and might give additional insight when deriving homogenization formulae. Also, we expect our conclusions to hold true for simplified EM models such as the 2.5D Maxwell's system [1].

The paper is organized as follows. In Section 1, we introduce Maxwell's equations and analyse the regularity of its solutions. We introduce the finite element spaces and carry out the error analysis in Section 2. Finally, numerical results are presented in Section 3, confirming our predicted convergence rates and the efficiency of the proposed methods.

1. Maxwell's equations

1.1. **Notation.** In this paper, $\Omega \subset \mathbb{R}^3$ is a bounded convex polyhedral open set. The symbol $\partial\Omega$ is used to denote the boundary of Ω, and $\mathbf{n}$ is the unit vector normal to $\partial\Omega$ and pointing outside Ω.

We assume that Ω is covered by a partition $\mathscr{P} = \{\Omega_k\}_{k=1}^S$ of polyhedron Ω_k. Then, the conductivity model $\sigma : \Omega \to \mathbb{R}_+^*$ takes one constant value σ_k on each Ω_k. We define $\sigma_\star = \min_k \sigma_k$ and $\sigma^\star = \max_k \sigma_k$. By assumption, we have $0 < \sigma_\star \leq \sigma^\star < +\infty$.

We denote $\mathcal{F}$ the set of faces related to the partition $\mathscr{P}$. For each face $F \in \mathcal{F}$ we define an associated normal vector $\mathbf{n}_F$ such that $\mathbf{n}_F = \mathbf{n}$ if $F \subset \partial\Omega$. Also, for each $k \in \{1, \ldots, S\}$, we denote by $\mathbf{n}_k$ the unit vector normal to $\partial\Omega_k$ and pointing outside Ω_k. The jump of σ through a face $F \in \mathcal{F}$ is defined as

$$[[\sigma]]_F = \begin{cases} (\sigma_k \mathbf{n}_k + \sigma_j \mathbf{n}_j) \cdot \mathbf{n}_F & \text{if } F = \partial\Omega_k \cap \partial\Omega_j, \\ \sigma_k & \text{if } F = \partial\Omega_k \cap \partial\Omega. \end{cases}$$

Throughout the rest of this document, symbol h will be reserved to denote the finite element mesh size. Also, $\beta \in (0, 1)$ will be a fixed constant representing the geometric regularity of the finite element mesh cells and $\delta > 0$ will be a strictly positive, arbitrarily small constant. If A, B are positive real numbers, we shall write $A \lesssim B$ if there exists a constant $C(\Omega, \mathscr{P}, \sigma, \beta, \delta)$ depending on Ω, $\mathscr{P}$, σ, β and δ, but independent of h, such that $A \leq C(\Omega, \mathscr{P}, \sigma, \beta, \delta)B$.

For an arbitrary open set $\mathcal{U} \subset \mathbb{R}^d$ with $d = 2$ or 3, $L^2(\mathcal{U})$ is the space of square integrable, complex-valued functions. For $s \in \mathbb{R}$, we classically denote by $H^s(\mathcal{U})$ the Sobolev space of complex-valued function defined in $\mathcal{U}$. We also introduce the spaces of vector functions $\mathbf{H}^s(\mathcal{U}) = (H^s(\mathcal{U}))^3$ and $\mathbf{L}^2(\mathcal{U}) = (L^2(\mathcal{U}))^3$. We use the notation $\|.\|_{s,\mathcal{U}}$ and $|.|_{s,\mathcal{U}}$ for the usual norm and semi-norm of $H^s(\mathcal{U})$ and $\mathbf{H}^s(\mathcal{U})$. The notation $(.,.)_{\mathcal{U}}$ is used for the $L^2(\mathcal{U})$ and $\mathbf{L}^2(\mathcal{U})$ inner-products. We drop the domain subscript if $\mathcal{U} = \Omega$. We refer the reader to [2, 25] for a discussion of these spaces.

If $\mathbf{u} \in \mathbf{L}^2(\mathcal{U})$, $\nabla \cdot \mathbf{u}$ and $\nabla \times \mathbf{u}$ denote its divergence and rotational in the sense of distributions, respectively. $\mathbf{H}(div, \mathcal{U})$ and $\mathbf{H}(curl, \mathcal{U})$ are the subspaces of $\mathbf{L}^2(\mathcal{U})$ having square integrable divergence and rotational, respectively [19]. These spaces are embedded with the norms

$$\|\mathbf{u}\|_{div,\mathcal{U}}^2 = |\mathbf{u}|_{0,\mathcal{U}}^2 + |\nabla \cdot \mathbf{u}|_{0,\mathcal{U}}^2, \quad \forall \mathbf{u} \in \mathbf{H}(div, \mathcal{U}),$$

and

$$\|\mathbf{u}\|_{curl,\mathcal{U}}^2 = |\mathbf{u}|_{0,\mathcal{U}}^2 + |\nabla \times \mathbf{u}|_{0,\mathcal{U}}^2, \quad \forall \mathbf{u} \in \mathbf{H}(curl, \mathcal{U}).$$

We denote by $\mathcal{D}(\mathcal{U})$ the space of C^∞ functions having compact support in $\mathcal{U}$. If $\mathcal{H}(\mathcal{U})$ is any of the aforementioned scalar (resp. vectorial) Sobolev spaces, then $\mathcal{H}_0(\mathcal{U})$ denotes the closure of $\mathcal{D}(\mathcal{U})$ (resp. $(\mathcal{D}(\mathcal{U}))^3$) in $\mathcal{H}(\mathcal{U})$.

Finally, for $s \in \mathbb{R}_+$, we shall also use "broken" Sobolev spaces of piecewise smooth functions onto the partition $\mathscr{P}$. These spaces are defined as

$$PH^s(\Omega, \mathscr{P}) = \left\{ u \in L^2(\Omega) \mid u \in H^s(\Omega_k) \; \forall \Omega_k \in \mathscr{P} \right\}$$

and $\mathbf{PH}^s(\Omega,\mathscr{P}) = (PH^s(\Omega))^3$. If $s < 1/2$, then $PH^s(\Omega,\mathscr{P}) = H^s(\Omega)$. For $s \geq 1/2$, if $u \in PH^s(\Omega,\mathscr{P})$ then $u \in H^{1/2-\delta}(\Omega)$. Analogous properties hold for the vectorial broken spaces [25].

1.2. **Model.** For a given electric source $\mathbf{J}$ and magnetic source $\mathbf{M}$, Maxwell's equations governing the electromagnetic fields for a nonzero frequency ω read

$$\left\{ \begin{array}{rcl} i\omega\mu_0\mathbf{H} - \nabla\times\mathbf{E} &=& \mathbf{M}, \\ \sigma\mathbf{E} + \nabla\times\mathbf{H} &=& \mathbf{J}, \end{array} \right. \tag{1}$$

in Ω. In addition, the following conditions are imposed on the boundary $\partial\Omega$:

$$\mathbf{E}\times\mathbf{n} = \mathbf{0}, \quad \mathbf{H}\cdot\mathbf{n} = 0. \tag{2}$$

In the above model, we assume that the permeability μ is constant and set to the vacuum value $\mu_0 = 4\pi\times 10^{-7} NA^{-2}$. Also, following [36], we assume that $\sigma + i\omega\varepsilon \simeq \sigma$, so that ε is set to zero. Actually, the only hypothesis that is mandatory on the parameters is that μ is constant. But to simplify notation in the proofs, we consider $\varepsilon = 0$.

We assume that all parameters are scalar valued, which corresponds to an isotropic propagation domain. This hypothesis is actually restrictive because most rocks are anisotropic. However, the isotropy hypothesis is mostly made to simplify the analysis (in particular, we can apply the results presented in [15]). Indeed, the extension of the proposed finite element method to anisotropic propagation media is straightforward.

As detailed before, the domain Ω is a convex polyhedron. In most geophysical applications, this hypothesis is rather realistic, because the boundary of the domain is not physical, but artificially designed to bound the computational domain. The size of the domain is related to the skin-depth relation [36], and the shape of the domain is generally a cube or a sphere-like polyhedron. For a non-convex domain, reentrant corners might generate singularities that are not considered in the present analysis. We refer the reader to [15, 8, 23, 30].

Assuming that $\mathbf{J},\mathbf{M} \in \mathbf{L}^2(\Omega)$, we can prove existence and uniqueness of weak solutions $\mathbf{E},\mathbf{H} \in \mathbf{H}(curl,\Omega)$ to (1)-(2) using the variational framework (see, for instance [27]). We recast the first-order system (1)-(2) into a second-order system, having only one unknown. As the original system features two unknowns, two choices are possible.

The electric field formulation is obtained by eliminating $\mathbf{H}$ from (1)-(2). Then, the equation for the electric field reads:

$$\left\{ \begin{array}{rcll} i\omega\mu_0\sigma\mathbf{E} + \nabla\times\nabla\times\mathbf{E} &=& i\omega\mu_0\mathbf{J} - \nabla\times\mathbf{M} & \text{in } \Omega \\ \mathbf{E}\times\mathbf{n} &=& \mathbf{0} & \text{on } \partial\Omega. \end{array} \right. \tag{3}$$

In the sense of distributions, boundary value problem (3) is equivalent to find $\mathbf{E} \in \mathbf{H}_0(curl,\Omega)$ such that

$$i\omega\mu_0(\sigma\mathbf{E},\mathbf{v}) + (\nabla\times\mathbf{E},\nabla\times\mathbf{v}) = i\omega\mu_0(\mathbf{J},\mathbf{v}) - (\mathbf{M},\nabla\times\mathbf{v}), \quad \forall\mathbf{v}\in\mathbf{H}_0(curl,\Omega). \tag{4}$$

Alternatively, for the magnetic field formulation, we look for $\mathbf{H} \in \mathbf{H}(curl,\Omega)$ satisfying

$$i\omega\mu_0(\mathbf{H},\mathbf{v}) + (\sigma^{-1}\nabla\times\mathbf{H},\nabla\times\mathbf{v}) = (\mathbf{M},\mathbf{v}) + (\sigma^{-1}\mathbf{J},\nabla\times\mathbf{v}), \quad \forall\mathbf{v}\in\mathbf{H}(curl,\Omega). \tag{5}$$

In order to shorten notation, we introduce the sesquilinear forms

$$b_{\mathbf{E}}(\mathbf{u},\mathbf{v}) = i\omega\mu_0(\sigma\mathbf{u},\mathbf{v}) + (\nabla\times\mathbf{u},\nabla\times\mathbf{v}), \quad \forall \mathbf{u},\mathbf{v}\in\mathbf{H}_0(curl,\Omega),$$

and

$$b_{\mathbf{H}}(\mathbf{u},\mathbf{v}) = i\omega\mu_0(\mathbf{u},\mathbf{v}) + (\sigma^{-1}\nabla\times\mathbf{u},\nabla\times\mathbf{v}), \quad \forall \mathbf{u},\mathbf{v}\in\mathbf{H}(curl,\Omega),$$

associated with (4) and (5).

We start by introducing some technical results that will be of use for the proofs of regularity of solutions.

1.3. **Technical preliminary results.** When analyzing the solutions of Maxwell's system (1), the variational theory easily shows that $\mathbf{E},\mathbf{H}\in\mathbf{H}(curl,\Omega)$ assuming that $\mathbf{J},\mathbf{M}\in\mathbf{L}^2(\Omega)$. A more subtle issue is to find optimal values $0<s,s'\leq 1$ such that $\mathbf{E}\in\mathbf{PH}^s(\Omega,\mathscr{P})$ and $\mathbf{H}\in\mathbf{PH}^{s'}(\Omega,\mathscr{P})$.

The exponents s,s' depend on the smoothness of the domain and the coefficients ε,μ and σ. In our settings, because μ is constant and Ω is convex, we can easily show that $\mathbf{H}\in\mathbf{H}^1(\Omega)$, so that $s'=1$. However, the regularity of $\mathbf{E}$ will be harder to analyse and we shall require technical results from [15, 8]. Here, the singularities of $\mathbf{E}$ are due to the conductivity parameter σ. Hence, we will denote by $\tau(\sigma)$ the highest value so that $\mathbf{E}\in\mathbf{PH}^s(\Omega,\mathscr{P})$ for all $0<s<\tau(\sigma)$. The characterization of $\tau(\sigma)$ is rather tricky [15, 8]. Nevertheless, we will give some insight of how $\tau(\sigma)$ might depend on σ.

The regularity of electric field is analysed through a Helmholtz-Hodge decomposition $\mathbf{E}=\boldsymbol{\phi}+\nabla p$, where $\boldsymbol{\phi}\in\mathbf{H}_0(curl,\Omega)$ is divergence free and $p\in H_0^1(\Omega)$. In our settings, it turns out that $\boldsymbol{\phi}\in\mathbf{H}^1(\Omega)$, so that the singularities of $\mathbf{E}$ are contained in p. Furthermore (see [15]), $p\in H_0^1(\Omega)$ can be characterized as the solution of a "Poisson type" variational problem:

$$(\sigma\nabla p,\nabla q) = (f,q) + \sum_{F\in\mathcal{F}}(g_F,q)_F \quad \forall q\in H_0^1(\Omega), \tag{6}$$

where $f\in L^2(\Omega)$ and $g_F\in H^{1/2}(F)$ for all $F\in\mathcal{F}$. And one can show [15] that

$$p\in PH^{1+s}(\Omega,\mathscr{P}) \tag{7}$$

for some $0<s\leq 1$. Then, $\tau(\sigma)$ is the highest value such that (7) holds for all $0<s<\tau(\sigma)$.

Boundary value problem (6) is rather unusual, because its right-hand-side involves surface sources on the interfaces of partition $\mathscr{P}$ and, as a result it does not belong to $L^2(\Omega)$. But Theorem 4.1 of [15] shows that the regularity of the solution p of (6) is the same as the regularity of $u\in H_0^1(\Omega)$ solution to

$$(\sigma\nabla u,\nabla v) = (f,v) \quad \forall v\in H_0^1(\Omega), \tag{8}$$

with $f\in L^2(\Omega)$. Hence, we can think of the electric field regularity as that of the gradient of a solution to the standard Poisson equation (8). Note that $\tau(\sigma)$ also corresponds to the convergence rates of a Lagrange finite element method in the H^1-norm, for the case of fitting meshes [9, Thm 9.25].

An important particular case occurs when the conductivity model is made of horizontal layers in a cubic domain. Indeed, in this configuration, we have $\tau(\sigma) = 2$ (for smooth enough right-hand side), and in particular $\mathbf{E} \in \mathbf{PH}^1(\Omega, \mathscr{P})$ (see [15]).

We also refer the reader to [8] for regularity results in more general domains and medium parameters.

1.4. **Electric field formulation.** We start with an existence and uniqueness result for (4). The analysis is greatly simplified because we assume that the conductivity is strictly positive. As a result, the proof of the following theorem relies simply on Lax-Milgram lemma and avoids the use of Fredholm alternative and compact embeddings (see Chapter 4 of [27]).

Theorem 1. *There exists a unique solution* $\mathbf{E} \in \mathbf{H}_0(curl, \Omega)$ *to* (4)*. Furthermore, it holds that*

$$\|\mathbf{E}\|_{curl} \lesssim |\mathbf{J}|_0 + |\mathbf{M}|_0. \tag{9}$$

Proof. If $\mathbf{v} \in \mathbf{H}_0(curl, \Omega)$, we have

$$b_{\mathbf{E}}(\mathbf{v}, \mathbf{v}) = i\omega\mu_0(\sigma\mathbf{v}, \mathbf{v}) + (\nabla \times \mathbf{v}, \nabla \times \mathbf{v}) = i\omega\mu_0|\sigma^{1/2}\mathbf{v}|_0^2 + |\nabla \times \mathbf{v}|_0^2,$$

and it follows that

$$|b_{\mathbf{E}}(\mathbf{v}, \mathbf{v})| \gtrsim \|\mathbf{v}\|_{curl}^2. \tag{10}$$

Inequality (10) implies that the sesquilinear form $b_{\mathbf{E}}$ is coercive. It is also easily seen that $b_{\mathbf{E}}$ is continuous. Finally, because $\mathbf{J}, \mathbf{M} \in \mathbf{L}^2(\Omega)$, the functional

$$\mathbf{H}_0(curl, \Omega) \ni \mathbf{v} \to i\omega\mu_0(\mathbf{J}, \mathbf{v}) - (\mathbf{M}, \nabla \times \mathbf{v}) \in \mathbb{C}$$

is an element of $(\mathbf{H}_0(curl, \Omega))'$. As a result, we can apply Lax-Milgram lemma (see, for instance Chapter 2 of [27]), and the existence and uniqueness of $\mathbf{E}$ follows.

To prove (9), we select $\mathbf{v} = \mathbf{E}$ in (4) and (10). Then, we have

$$\|\mathbf{E}\|_{curl}^2 \lesssim |b_{\mathbf{E}}(\mathbf{E}, \mathbf{E})| = |i\omega\mu_0(\mathbf{J}, \mathbf{E}) - (\mathbf{M}, \nabla \times \mathbf{E})| \lesssim (|\mathbf{J}|_0 + |\mathbf{M}|_0)\|\mathbf{E}\|_{curl}.$$

□

Now, we show that if additional regularity is assumed on $\mathbf{J}$ and/or $\mathbf{M}$, additional regularity can be expect for the electric field. The proof involves the exponent $\tau(\sigma)$ associated with Poisson equation that is introduced in Subsection 1.3.

Theorem 2. *If* $\mathbf{J} \in \mathbf{H}(div, \Omega)$*, then* $\mathbf{E} \in \mathbf{PH}^s(\Omega, \mathscr{P})$ *and it holds that*

$$\sum_{k=1}^{S} |\mathbf{E}|_{s,\Omega_k} \lesssim \|\mathbf{J}\|_{div} + |\mathbf{M}|_0, \tag{11}$$

for all $0 < s < \tau(\sigma)$*. Also* $\mathbf{E} \in \mathbf{H}^t(\Omega)$

$$|\mathbf{E}|_t \lesssim \|\mathbf{J}\|_{div} + |\mathbf{M}|_0, \tag{12}$$

for all $0 < t < \tilde{\tau}(\sigma) = \min(\tau(\sigma), 1/2)$.

If $\mathbf{M} \in \mathbf{H}(curl, \Omega)$*, then* $\nabla \times \mathbf{E} \in \mathbf{H}^1(\Omega)$ *and it holds that*

$$|\nabla \times \mathbf{E}|_1 \lesssim |\mathbf{J}|_0 + \|\mathbf{M}\|_{curl}. \tag{13}$$

Proof. In order to prove (11), we first introduce the Hodge-Helmholtz decomposition

$$\mathbf{E} = \nabla p + \boldsymbol{\psi},$$

where $\boldsymbol{\psi} \in \mathbf{H}_0(curl, \Omega)$ is such that $\nabla \cdot \boldsymbol{\psi} = 0$, and $p \in H_0^1(\Omega)$ is solution to

$$(\sigma \nabla p, \nabla q) = (\mathbf{J} - \sigma \boldsymbol{\psi}, \nabla q), \quad \forall q \in H_0^1(\Omega). \tag{14}$$

Theorem I.3.7 of [19] ensures that $\boldsymbol{\psi} \in \mathbf{H}^1(\Omega)$ and $\|\boldsymbol{\psi}\|_1 \lesssim |\nabla \times \mathbf{E}|_0$. Hence, it remains to study the regularity of p. We will show that $p \in PH^{1+s}(\Omega, \mathscr{P})$ and

$$\sum_{k=1}^{S} |p|_{1+s,\Omega_k} \lesssim |\nabla \cdot \mathbf{J}|_0 + |\nabla \times \mathbf{E}|_0,$$

for all $0 < s < \tau(\sigma)$, which proves equation (11), since $|\nabla \times \mathbf{E}|_0$ has already been bounded in Theorem 1.

Since $\boldsymbol{\psi} \in \mathbf{H}^1(\Omega)$, by applying Green's formula in each Ω_k, we have

$$\begin{aligned} (\sigma \boldsymbol{\psi}, \nabla q) &= \sum_{k=1}^{S} \sigma_k \int_{\Omega_k} \boldsymbol{\psi} \cdot \nabla q \\ &= \sum_{k=1}^{S} \sigma_k \left\{ \int_{\partial \Omega_k} \boldsymbol{\psi} \cdot \mathbf{n}_K q - \int_{\Omega_k} \nabla \cdot \boldsymbol{\psi} q \right\}. \end{aligned}$$

Because $\nabla \cdot \boldsymbol{\psi} = 0$, the second term vanishes. Furthermore, we can rearrange the first term so that

$$(\sigma \boldsymbol{\psi}, \nabla q) = \sum_{F \in \mathcal{F}} [[\sigma]]_F \int_F \boldsymbol{\psi} \cdot \mathbf{n}_F q.$$

We thus find that $p \in H_0^1(\Omega)$ is solution to

$$(\sigma \nabla p, \nabla q) = (f, q) + \sum_{F \in \mathcal{F}} (g_F, q)_F, \quad \forall q \in H_0^1(\Omega),$$

with $f = -\nabla \cdot J \in L^2(\Omega)$ and $g_F = -[[\sigma]]_F \boldsymbol{\psi} \cdot \mathbf{n}_F \in H^{1/2}(F)$ for all $F \in \mathcal{F}_{int}$.

Recalling Subsection 1.3, it follows that for $0 < s < \tau(\sigma)$, $p \in PH^{1+s}(\Omega, \mathscr{P})$, with

$$\sum_{k=1}^{S} |p|_{1+s,\Omega_k} \lesssim |\nabla \cdot \mathbf{J}|_0 + \sum_{F \in \mathcal{F}_{\text{int}}} [[\sigma]]_F \|\boldsymbol{\psi} \cdot \mathbf{n}_F\|_{0,F}.$$

Therefore, by a trace theorem, we obtain

$$\sum_{k=1}^{S} |p|_{1+s,\Omega_k} \lesssim |\nabla \cdot \mathbf{J}|_0 + \|\boldsymbol{\psi}\|_1,$$

and we recover (11) by the previous estimate on $\|\boldsymbol{\psi}\|_1$.

Recalling that $\tilde{\tau}(\sigma) = \min(\tau(\sigma), 1/2)$, we have $\tilde{\tau}(\sigma) \leq \tau(\sigma)$ so that $\mathbf{E} \in \mathbf{PH}^t(\Omega, \mathscr{P})$ for all $0 < t < \tilde{\tau}(\sigma)$. As $\tilde{\tau}(\sigma) < 1/2$, we have $\mathbf{PH}^t(\Omega, \mathscr{P}) = \mathbf{H}^t(\Omega)$, and (12) follows.

We now prove (13). In order to simplify notation, we write $\boldsymbol{\phi} = \nabla \times \mathbf{E} \in \mathbf{L}^2(\Omega)$. Assuming that $\mathbf{M} \in \mathbf{H}(curl, \Omega)$, we can write from (4) that

$$(\boldsymbol{\phi}, \nabla \times \mathbf{v}) = (-i\omega\mu_0\sigma\mathbf{E} + i\omega\mu_0\mathbf{J} - \nabla \times \mathbf{M}, \mathbf{v}), \quad \forall \mathbf{v} \in \mathbf{H}_0(curl, \Omega).$$

As a result, we have $\nabla \times \boldsymbol{\phi} \in \mathbf{L}^2(\Omega)$ and

$$|\nabla \times \boldsymbol{\phi}|_0 \leq \omega\mu_0\sigma^\star|\mathbf{E}|_0 + \omega\mu_0|\mathbf{J}|_0 + |\nabla \times \mathbf{M}|_0.$$

From (9), it follows that

$$|\nabla \times \boldsymbol{\phi}|_0 \lesssim |\mathbf{J}|_0 + |\mathbf{M}|_0 + |\nabla \times \mathbf{M}|_0.$$

As $\boldsymbol{\phi} = \nabla \times \mathbf{E}$, we have $\nabla \cdot \boldsymbol{\phi} = 0$ on Ω and $\boldsymbol{\phi} \cdot \mathbf{n} = 0$ on $\partial\Omega$. Hence, applying Theorem I.3.9 from [19], we obtain (13). □

1.5. **Magnetic field formulation.** In the previous subsection, we have reformulated the first-order system (1)-(2) into second-order boundary value problem (4) in terms of the electric field. In this subsection, we study the analogous formulation (5) in terms of the magnetic field.

In Theorem 3, we state an existence and uniqueness result for the magnetic field. The proof is similar to the electric field formulation and it is not reproduced here.

Theorem 3. *There exists a unique solution* $\mathbf{H} \in \mathbf{H}(curl, \Omega)$ *to* (5)*. Furthermore, it holds that*

$$\|\mathbf{H}\|_{curl} \lesssim |\mathbf{J}|_0 + |\mathbf{M}|_0. \tag{15}$$

Following the analysis of the electric field formulation, we show that if additional regularity is assumed on $\mathbf{J}$ and/or $\mathbf{M}$, the regularity of $\mathbf{H}$ is improved. Here again, the exponent $\tau(\sigma)$ defined earlier plays a crucial role.

Theorem 4. *If* $\mathbf{M} \in \mathbf{H}_0(div, \Omega)$*, then* $\mathbf{H} \in \mathbf{H}^1(\Omega)$*, and it holds that*

$$|\mathbf{H}|_1 \lesssim |\mathbf{J}|_0 + \|\mathbf{M}\|_{div}. \tag{16}$$

If $\sigma^{-1}\mathbf{J} \in \mathbf{H}_0(curl, \Omega)$*, then* $\nabla \times \mathbf{H} \in \mathbf{PH}^s(\Omega)$*, and it holds that*

$$\sum_{k=1}^{S} |\nabla \times \mathbf{H}|_{s,\Omega_k} \lesssim \|\sigma^{-1}\mathbf{J}\|_{curl} + |\mathbf{M}|_0, \tag{17}$$

for all $0 < s < \tau(\sigma)$*. Consequently* $\nabla \times \mathbf{H} \in \mathbf{H}^t(\Omega)$ *and*

$$|\nabla \times \mathbf{H}|_t \lesssim \|\sigma^{-1}\mathbf{J}\|_{curl} + |\mathbf{M}|_0, \tag{18}$$

for all $0 < t < \tilde{\tau}(\sigma) = \min(\tau(\sigma), 1/2)$*.*

Proof. We first show (16). Taking $\mathbf{v} = \nabla p$ with $p \in H^1(\Omega)$ in (5), we have that

$$(\mathbf{H}, \nabla p) = (\mathbf{M}, \nabla p).$$

Since $\mathbf{M} \in \mathbf{H}_0(div,\Omega)$, then $\mathbf{H} \in \mathbf{H}_0(div,\Omega)$ and $\nabla\cdot\mathbf{H} = \nabla\cdot\mathbf{M} \in L^2(\Omega)$. Recalling (15), we also have that $\nabla\times\mathbf{H} \in \mathbf{L}^2(\Omega)$, and (16) follows from Theorem I.3.9 of [19].

In order to prove (17), we define $\mathbf{R} = \sigma^{-1}\nabla\times\mathbf{H}$. Since $\mathbf{H} \in \mathbf{H}(curl,\Omega)$ and $\sigma^{-1} \leq \sigma_\star^{-1} < +\infty$, we have $\mathbf{R} \in \mathbf{L}^2(\Omega)$. Furthermore, because $\nabla\times(\sigma^{-1}\mathbf{J}) \in \mathbf{H}_0(curl,\Omega)$, a simple manipulation of (5) shows that

$$(\mathbf{R}, \nabla\times\mathbf{v}) = (\mathbf{M} + \nabla\times(\sigma^{-1}\mathbf{J}) - i\omega\mu_0\mathbf{H}, \mathbf{v}) \quad \forall\mathbf{v} \in \mathbf{H}(curl,\Omega). \tag{19}$$

It follows that $\mathbf{R} \in \mathbf{H}_0(curl,\Omega)$. Let us introduce the Hodge-Helmholtz decomposition $\mathbf{R} = \boldsymbol{\psi} + \nabla p$, where $\boldsymbol{\psi} \in \mathbf{H}_0(curl,\Omega)$ satisfies $\nabla\cdot\boldsymbol{\psi} = 0$ and $p \in H_0^1(\Omega)$.

Since Ω is convex, Theorem I.3.7 of [19] ensures that $\boldsymbol{\psi} \in \mathbf{H}^1(\Omega)$ and $\|\boldsymbol{\psi}\|_1 \lesssim |\nabla\times\mathbf{R}|_0$. Recalling (19) and (15), it follows that

$$\|\boldsymbol{\psi}\|_1 \lesssim \|\sigma^{-1}\mathbf{J}\|_{curl} + |\mathbf{M}|_0.$$

It remains to analyse p, which contains the singularities. To do so, we observe that since $\sigma\mathbf{R} = \nabla\times\mathbf{H}$, we have $(\sigma\mathbf{R}, \nabla q) = 0$, for all $q \in H_0^1(\Omega)$. As a result, we see that p is the unique solution in $H_0^1(\Omega)$ of

$$(\sigma\nabla p, \nabla q) = -(\sigma\boldsymbol{\psi}, \nabla q). \tag{20}$$

We now apply the same transformation to the right-hand-side of (20) than in Theorem 2 to show that p is actually solution to

$$(\sigma\nabla p, \nabla q) = -\sum_{F\in\mathcal{F}} [[\sigma]]_F(\boldsymbol{\psi}\cdot\mathbf{n}_F, q)_F \quad \forall q \in H_0^1(\Omega),$$

and it follows (see Subsection 1.3) that $\mathbf{R} \in \mathbf{PH}^s(\Omega,\mathscr{P})$ and

$$\sum_{k=1}^{S} |\mathbf{R}|_{s,\Omega_k} \lesssim \sum_{F\in\mathcal{F}} \|\boldsymbol{\psi}\|_{1/2,F} \lesssim \|\boldsymbol{\psi}\|_1,$$

for all $0 < s < \tau(\sigma)$.

Finally (17) follows since $\nabla\times\mathbf{H} = \sigma\mathbf{R}$ and σ is constant on each $\Omega_k \in \mathscr{P}$ by construction. □

2. Finite-element discretization

2.1. **Settings.** The finite element spaces we use consist of the standard Nédélec's edge elements [29]. Because we work with low-regularity fields, we will employ special "quasi-interpolation" operators defined in [35]. These operators are rigorously analysed for tetrahedral meshes only. As a result, our theoretical analysis is carried out for tetrahedral meshes. Nevertheless, we expect all our results to hold for cartesian grid meshes with cubic cells. The missing part in the proofs would be to extend the work from [35] to cubic elements.

Hence, we introduce a family of tetrahedral meshes $\mathcal{T}_h = \{K\}$ of Ω, with parameter $h > 0$. We assume that this family of meshes is regular in the sense of [13]. That is, every mesh is conforming, which means that the intersection of two cells $\overline{K_+} \cap \overline{K_-}$ is either a

full face, a full edge or a node of the two cells. Additionally, each cell $K \in \mathcal{T}_h$ is a "shape regular" tetrahedra, i.e. it satisfies

$$\operatorname{diam} K \leq h, \quad \frac{\rho(K)}{\operatorname{diam} K} \geq \beta,$$

where $\beta \in (0,1)$ is a h-independent constant and

$$\rho(K) = \sup\{r > 0 \mid \exists \mathbf{x} \in K,\ B(\mathbf{x}, r) \subset K\}, \quad \operatorname{diam}(K) = \sup\{|\mathbf{x} - \mathbf{y}| \mid \mathbf{x}, \mathbf{y} \in K\}.$$

We say that a mesh $\mathcal{T}_h$ is a $\mathscr{P}$-fitting mesh (or simply, a fitting mesh) if

$$\forall K \in \mathcal{T}_h,\ \exists \Omega_k \in \mathscr{P} \text{ such that } K \subset \Omega_k. \tag{21}$$

On the other hand, a mesh that does not satisfy (21) will be called a non $\mathscr{P}$-fitting mesh (or simply, a non-fitting mesh).

For a given $h > 0$, the space of first-order Nédélec's element space is defined in [29] as

$$\mathbf{V}_h = \{\mathbf{v}_h \in H(curl, \Omega) \mid \mathbf{v}_h|_K \in \mathcal{R}(K), \quad \forall K \in \mathcal{T}_h\},$$

where

$$\mathcal{R}(K) = \{\mathbf{v} \in \mathcal{P}_1(K)^3 \mid \nabla \mathbf{v} + (\nabla \mathbf{v})^T = 0\}.$$

While the space $\mathbf{V}_h$ is actually used to approximate the magnetic field, it misses the essential boundary conditions of the electric field. Thus, in order to approximate the electric field, we further introduce

$$\mathbf{V}_{h,0} = \mathbf{V}_h \cap \mathbf{H}_0(curl, \Omega) = \{\mathbf{v}_h \in \mathbf{V}_h \mid \mathbf{v}_h \times \mathbf{n} = 0 \text{ on } \partial\Omega\}.$$

We also introduce the space S^h of Lagrange finite elements, defined by

$$S^h = \left\{q^h \in H^1(\Omega) \mid q^h|_K \in \mathcal{P}_1(K) \quad \forall K \in \mathcal{T}_h\right\},$$

and

$$S_0^h = S^h \cap H_0^1(\Omega) = \left\{q^h \in S^h \mid q^h = 0 \text{ on } \partial\Omega\right\}.$$

It is easily seen that, if $q^h \in S^h$ (resp. if $q^h \in S_0^h$), then $\nabla q^h \in \mathbf{V}_h$ (resp. $\nabla q^h \in \mathbf{V}_{h,0}$).

For sufficiently regular functions $\mathbf{v} : \Omega \to \mathbb{C}^3$ and $q : \Omega \to \mathbb{C}$, it is customary to introduce the edge and the nodal interpolant $\Pi_h \mathbf{v} \in \mathbf{V}_h$ and $r^h(q) \in S^h$. The edge interpolant was first designed by Nédélec [29] for regular fields $\mathbf{v} \in \mathbf{H}^2(\Omega)$ and the definition was later extended in [16] for fields $\mathbf{v} \in \mathbf{H}^1(\Omega)$ such that $\nabla \times \mathbf{v} \in \mathbf{H}^1(\Omega)$. Similarly, the nodal interpolant requires the function q to be continuous [13], as a result it is well defined if $q \in H^2(\Omega)$.

Since we work with low regularity fields, the aforementioned interpolation operators are insufficient. A review of interpolation theory for low regularity electromagnetic fields is given in [23]. Here after, we will use "quasi-interpolation" operators defined in [35], which are well-defined when $\mathbf{v} \in \mathbf{L}^2(\Omega)$ and $q \in L^2(\Omega)$.

We summarize the results we shall require in Propositions 1 and 2. The quasi-interpolation operators are extensively described in [35], where the proofs of the two propositions can be found (strictly speaking, the proofs are only presented for the case $t = t' = 1$, but the results naturally extend for $t, t' \in [0, 1]$).

Proposition 1. *For all* $\mathbf{v} \in \mathbf{L}^2(\Omega)$*, there exists an element* $\Pi_{h,0}\mathbf{v} \in \mathbf{V}_{h,0}$ *such that*

$$\|\Pi_{h,0}\mathbf{v}\|_{curl} \lesssim |\mathbf{v}|_0.$$

Furthermore, for all cells $K \in \mathcal{T}_h$*, if* $\mathbf{v} \in \mathbf{H}^t(K)$ *for some* $t \in [0,1]$*, then it holds*

$$|\mathbf{v} - \Pi_{h,0}\mathbf{v}|_{0,K} \lesssim h^t |\mathbf{v}|_{t,K}, \tag{22}$$

while if $\nabla \times \mathbf{v} \in \mathbf{H}^{t'}(K)$ *for some* $t' \in [0,1]$*, we have*

$$|\nabla \times (\mathbf{v} - \Pi_{h,0}\mathbf{v})|_{0,K} \lesssim h^{t'} |\nabla \times \mathbf{v}|_{t',K}. \tag{23}$$

Finally, if $\mathbf{v} = \nabla q$ *for some* $q \in H_0^1(\Omega)$*, then there exists an element* $r_0^h(q) \in S_0^h$ *such that*

$$\Pi_{h,0}(\nabla q) = \nabla r_0^h(q).$$

In Proposition 2, we introduce the quasi-interpolation operator Π_h, which is the analogue of $\Pi_{h,0}$ for the space $\mathbf{V}_h$.

Proposition 2. *For all* $\mathbf{v} \in \mathbf{L}^2(\Omega)$*, there exists an element* $\Pi_h\mathbf{v} \in \mathbf{V}_h$ *such that*

$$\|\Pi_h\mathbf{v}\|_{curl} \lesssim |\mathbf{v}|_0.$$

Furthermore, for all cells $K \in \mathcal{T}_h$*, if* $\mathbf{v} \in \mathbf{H}^t(K)$ *for some* $t \in [0,1]$*, then it holds*

$$|\mathbf{v} - \Pi_h\mathbf{v}|_{0,K} \lesssim h^t |\mathbf{v}|_{t,K}, \tag{24}$$

while if $\nabla \times \mathbf{v} \in \mathbf{H}^{t'}(K)$ *for some* $t' \in [0,1]$*, we have*

$$|\nabla \times (\mathbf{v} - \Pi_h\mathbf{v})|_{0,K} \lesssim h^{t'} |\nabla \times \mathbf{v}|_{t',K}. \tag{25}$$

Finally, if $\mathbf{v} = \nabla q$ *for some* $q \in H^1(\Omega)$*, then there exists* $r^h(q) \in S^h$ *such that*

$$\Pi_h(\nabla q) = \nabla r^h(q). \tag{26}$$

2.2. **A discussion on fitting and non-fitting meshes.** As depicted on Figure 1, non-fitting meshes have interesting applications, as they can simplify implementations and/or reduce computational costs. Unfortunately, they also come with additional difficulties that we shall discuss in this subsection. These complications occur because material discontinuities are allowed inside mesh cells. As a result, the normal component of the electric field jumps through the interface inside mesh cells, so that a discontinuous function must be approximated by continuous finite element shape functions. Also, numerical integration becomes more challenging.

We will describe these two issues and explain precisely what are the implications and the possible solutions. For simplicity, we only analyse the electric field formulation in this discussion. However, all our remarks remain unchanged for the magnetic field formulation.

2.2.1. *Linear system assembling.* The finite element linear system associated with variational formulation (4) has entries given by $M_{ij} = b_{\mathbf{E}}(\phi_j, \phi_i)$ where $\phi_i, \phi_j \in \mathbf{V}_{h,0}$ are finite element shape functions. In particular, it is required to compute the quantities

$$\int_K \sigma \phi_j \cdot \phi_i, \tag{27}$$

where K is a mesh cell. When a fitting mesh is used, σ takes one constant value σ_K on K, so that computing (27) amounts to integrate a polynomial function onto a tetrahedra. This can be done analytically, and optimized techniques using affine mappings can be used to do it efficiently [13, 27]. When the mesh does not fit the conductivity model, additional techniques are required [11]. Fortunately, as shown in [6], an efficient and accurate technique has been developed. Briefly speaking, the key idea is to introduce an approximation σ_ϵ to σ such that

$$\int_K \sigma_\epsilon \phi_j \cdot \phi_i,$$

is easily computed and is a good approximation to (27). As a result, this first issue can be resolved with an easily-implemented strategy.

2.2.2. *Convergence rates.* The second problem is due to the lack of regularity of the solution inside the mesh cells. In terms of Sobolev spaces, the accuracy of the finite element solution is directly related to the regularity of the solution inside each cell. For instance $\mathbf{E}|_K \in \mathbf{H}^s(K)$ for some $0 < s \leq 1$ where $K \in \mathcal{T}_h$ is a mesh cell.

If the mesh is $\mathcal{P}$-fitting, then each cell $K \in \mathcal{T}_h$ is included inside one subdomain $\Omega_k \in \mathscr{P}$. As a result, $K \subset \Omega_k$ and $\mathbf{E} \in \mathbf{PH}^s(\Omega, \mathscr{P})$ implies that $\mathbf{E}|_K \in \mathbf{H}^s(K)$ for all $0 < s < \tau(\sigma)$. On the other hand, if the mesh does not fit the partition $\mathscr{P}$, then we only have $\mathbf{E}|_K \in \mathbf{H}^t(K)$ for $0 < t < \tilde{\tau}(\sigma) = \min(\tau(\sigma), 1/2)$. Thus, in the absence of singularity, or more generally if $\tau(\sigma) > 1/2$, we can not expect non-fitting meshes to be as accurate as fitting meshes, because the electric field is less regular inside each cell. Indeed, we will show that the convergence rate of the electric field approximation in the L^2-norm is $\mathcal{O}(h^{\tau(\sigma)})$ for fitting meshes and only $\mathcal{O}(h^{\tilde{\tau}(\sigma)})$ for non-fitting meshes.

In order to illustrate this point, let us consider the case of a cubic domain with plane horizontal interfaces. Then according to [15], we have $\mathbf{E} \in \mathbf{PH}^1(\Omega, \mathscr{P})$ and, if $\mathcal{T}_h$ is a fitting mesh, then $\mathbf{E}|_K \in \mathbf{H}^1(K)$ for all $K \in \mathcal{T}_h$. It follows that the convergence rate of Nédélec's finite element will be linear if fitting meshes are used. However, for a non-fitting mesh, we only have $\mathbf{E}|_K \in \mathbf{H}^{(1-\delta)/2}(K)$, since the vertical component of $\mathbf{E}$ might jump inside K (recalling Subsection 1.1, $\delta > 0$ is an arbitrarily small constant). As a result, the convergence rate of Nédélec's finite elements with non-fitting meshes will be at most $\mathcal{O}(h^{(1-\delta)/2})$.

The main novelty of our analysis is that when the permeability is constant, the approximations of the electric and magnetic fields have different convergence rates. Indeed, we are able to show that the if the electric field converges as $\mathcal{O}(h^s)$, then the magnetic field error decreases as $\mathcal{O}(h^{\min(1,2s)})$. For a cubic domain with horizontal layers, it means that the magnetic field approximation on a non-fitting mesh will converge as $\mathcal{O}(h^{(1-\delta)})$. As a

result, the observed convergence rate is linear, just as in the case of fitting meshes. More generally, it implies that fitting and non-fitting meshes will provide the same convergence rate for the magnetic field error in the L^2-norm: $\mathcal{O}(h^{\min(1,2s)})$, where $0 < s < \tau(\sigma)$.

Thus, our main claim is that if non-fitting meshes do imply an accuracy loss concerning the electric field approximation, they provide the same convergence rate that fitting meshes for the magnetic field approximation. In the following subsections, we support this claim with rigorous proofs, both for the electric and magnetic field formulations of Maxwell's equations.

2.3. **The electric field formulation.** We first discretize the electric field formulation (4). In this case, we seek a Galerkin approximation $\mathbf{E}_h$ to $\mathbf{E}$ in the space $\mathbf{V}_{h,0}$. As usual, the approximation is defined using the discrete variational problem: Find $\mathbf{E}_h \in \mathbf{V}_{h,0}$ such that

$$b_{\mathbf{E}}(\mathbf{E}_h, \mathbf{v}_h) = i\omega\mu_0(\mathbf{J}, \mathbf{v}_h) - (\mathbf{M}, \nabla \times \mathbf{v}_h) \quad \forall \mathbf{v}_h \in \mathbf{V}_{h,0}. \tag{28}$$

Solving (28) amounts to factorizing a linear system. Then, the discrete representation of the magnetic field $\mathbf{H}_h$ is obtained by post-processing as

$$\mathbf{H}_h = \frac{1}{i\omega\mu_0}\left(\mathbf{M} + \nabla \times \mathbf{E}_h\right). \tag{29}$$

From (29), it is clear that the error committed on the approximation of the magnetic field in the L^2-norm is proportional to $|\nabla \times (\mathbf{E} - \mathbf{E}_h)|_0$. Thus, we will speak of "magnetic field" error to denote $|\nabla \times (\mathbf{E} - \mathbf{E}_h)|_0$. On the other hand, we will name "electric field" error the quantity $|\mathbf{E} - \mathbf{E}_h|_0$.

In view of Theorem 2, in all this subsection, we require that $\mathbf{J} \in \mathbf{H}(div, \Omega)$ and $\mathbf{M} \in \mathbf{H}(curl, \Omega)$.

2.3.1. *Interpolation error estimates.* In order to simplify the following proofs, let us define, for arbitrary $\mathbf{j}, \mathbf{m} \in \mathbf{L}^2(\Omega)$, $\mathcal{E}(\mathbf{j}, \mathbf{m}) \in \mathbf{H}_0(curl, \Omega)$ as the solution to

$$b_{\mathbf{E}}(\mathcal{E}(\mathbf{j}, \mathbf{m}), \mathbf{v}) = i\omega\mu_0(\mathbf{j}, \mathbf{v}) - (\mathbf{m}, \nabla \times \mathbf{v}), \quad \forall \mathbf{v} \in \mathbf{H}_0(curl, \Omega).$$

In particular, $\mathbf{E} = \mathcal{E}(\mathbf{J}, \mathbf{M})$, and Theorems 1 and 2 hold if $\mathbf{E}$, $\mathbf{J}$ and $\mathbf{M}$ are replaced by $\mathcal{E}(\mathbf{j}, \mathbf{m})$, $\mathbf{j}$ and $\mathbf{m}$, respectively.

Later, we will need to quantify, for arbitrary right-hand-sides $\mathbf{j}, \mathbf{m} \in \mathbf{L}^2(\Omega)$, the ability of the interpolant $\Pi_{h,0}\mathcal{E}(\mathbf{j}, \mathbf{m})$ to approximate the solution $\mathcal{E}(\mathbf{j}, \mathbf{m})$. Hence, we introduce, for $h > 0$

$$\eta_h^{\mathbf{E}} = \sup_{\mathbf{j} \in \mathbf{H}(div,\Omega), \mathbf{m} \in \mathbf{L}(\Omega)^3} \frac{|\mathcal{E}(\mathbf{j}, \mathbf{m}) - \Pi_{h,0}\mathcal{E}(\mathbf{j}, \mathbf{m})|_0}{\|\mathbf{j}\|_{div} + |\mathbf{m}|_0},$$

and

$$\eta_h^{\mathbf{H}} = \sup_{\mathbf{j} \in \mathbf{L}^2(\Omega), \mathbf{m} \in \mathbf{H}(curl,\Omega)} \frac{|\nabla \times (\mathcal{E}(\mathbf{j}, \mathbf{m}) - \Pi_{h,0}\mathcal{E}(\mathbf{j}, \mathbf{m}))|_0}{|\mathbf{j}|_0 + \|\mathbf{m}\|_{curl}}.$$

The quantities $\eta_h^{\mathbf{E}}$ and $\eta_h^{\mathbf{H}}$ control the interpolation error on the electric and magnetic fields, respectively, since by definition, we have

$$|\mathcal{E}(\mathbf{j}, \mathbf{m}) - \Pi_{h,0}\mathcal{E}(\mathbf{j}, \mathbf{m})|_0 \lesssim \eta_h^{\mathbf{E}}\left(\|\mathbf{j}\|_{div} + |\mathbf{m}|_0, \right), \quad \forall \mathbf{j} \in \mathbf{H}(div, \Omega),\ \forall \mathbf{m} \in \mathbf{L}^2(\Omega),$$

and

$$|\nabla \times (\mathcal{E}(\mathbf{j},\mathbf{m}) - \Pi_{h,0}\mathcal{E}(\mathbf{j},\mathbf{m}))|_0 \lesssim \eta_h^{\mathbf{E}} \left(|\mathbf{j}|_0 + \|\mathbf{m}\|_{curl}\right), \quad \forall \mathbf{j} \in \mathbf{L}^2(\Omega),\ \forall \mathbf{m} \in \mathbf{H}(curl,\Omega).$$

In the following theorem, we bound the quantities $\eta_h^{\mathbf{E}}$ and $\eta_h^{\mathbf{H}}$. We observe that the $\mathscr{P}$-fitting property impacts the behaviour of $\eta_h^{\mathbf{E}}$, but not that of $\eta_h^{\mathbf{H}}$.

Theorem 5. *It holds that*

$$\eta_h^{\mathbf{H}} \lesssim h, \tag{30}$$

whether or not the mesh is $\mathscr{P}$-fitting.

If $\mathcal{T}_h$ is a $\mathscr{P}$-fitting mesh, then we have

$$\eta_h^{\mathbf{E}} \lesssim h^s, \tag{31}$$

for all $0 < s < \tau(\sigma)$.

If $\tilde{\mathcal{T}}_h$ is a non $\mathscr{P}$-fitting mesh, we only have

$$\eta_h^{\mathbf{E}} \lesssim h^t, \tag{32}$$

for all $0 < t < \tilde{\tau}(\sigma)$.

Proof. In view of (22) and (23), it is clear that the key element is the regularity of $\mathcal{E}(\mathbf{j},\mathbf{m})|_K$ and $\nabla \times \mathcal{E}(\mathbf{j},\mathbf{m})|_K$ for an arbitrary cell $K \in \mathcal{T}_h$ or $\tilde{\mathcal{T}}_h$.

Let $\mathbf{j} \in \mathbf{L}^2(\Omega)$ and $\mathbf{m} \in \mathbf{H}(curl,\Omega)$. Recalling (13), we have $\nabla \times \mathcal{E}(\mathbf{j},\mathbf{m}) \in \mathbf{H}^1(\Omega)$ so that $\mathcal{E}(\mathbf{j},\mathbf{m})|_K \in \mathbf{H}^1(K)$ for all $K \in \mathcal{T}_h \cup \tilde{\mathcal{T}}_h$. It follows that $\eta_h^{\mathbf{H}} \lesssim h$ by summing (23) over all $K \in \mathcal{T}_h$ (resp. $\tilde{\mathcal{T}}_h$) and applying (13).

Now, let $\mathbf{j} \in \mathbf{H}(div,\Omega)$ and $\mathbf{m} \in \mathbf{L}^2(\Omega)$. From (11), we have $\mathcal{E}(\mathbf{j},\mathbf{m}) \in \mathbf{PH}^s(\Omega,\mathscr{P})$ for $0 < s < \tau(\sigma)$. If $\mathcal{T}_h$ is $\mathscr{P}$-fitting, it follows that $\mathcal{E}(\mathbf{j},\mathbf{m})|_K \in \mathbf{H}^s(K)$ for all $K \in \mathcal{T}_h$ and we conclude from (22) and (11) that $\eta_h^{\mathbf{E}} \lesssim h^s$.

If $K \in \mathcal{T}_h$, we do not have $\mathcal{E}(\mathbf{j},\mathbf{m})|_K \in \mathbf{H}^s(K)$ for all $0 < s < \tau(\sigma)$ when $\mathcal{T}_h$ is non $\mathcal{P}$-fitting. However, since it holds that $\mathcal{E}(\mathbf{j},\mathbf{m}) \in \mathbf{H}^t(\Omega)$ for $0 < t < \tilde{\tau}(\sigma)$, we obtain that $\eta_h^{\mathbf{E}} \lesssim h^t$ from (22) and (11). □

2.3.2. *Electric field error estimates.* We see from (22) and (23) that the interpolation error in the L^2-norm is smaller for the magnetic field than for the electric field. Unfortunately, as shown in Theorem 6, a direct application of Céa's lemma gives the same convergence rate for both electromagnetic fields. Hence, the improved accuracy of the interpolant for the magnetic field stays hidden.

Theorem 6. *For all $h > 0$, there exists a unique $\mathbf{E}_h \in \mathbf{V}_{h,0}$ solution to* (28)*. Furthermore, the discrete solution $\mathbf{E}_h$ satisfies*

$$\|\mathbf{E} - \mathbf{E}_h\|_{curl} \lesssim \left(\eta_h^{\mathbf{E}} + \eta_h^{\mathbf{H}}\right) \left(\|\mathbf{J}\|_{div} + \|\mathbf{M}\|_{curl}\right). \tag{33}$$

Proof. Since $b_{\mathbf{E}}$ is coercive, the proof is a simple application of Céa's lemma. Indeed, by Galerkin orthogonality, we have

$$\begin{aligned} \|\mathbf{E}-\mathbf{E}_h\|_{curl}^2 &\lesssim |b_{\mathbf{E}}(\mathbf{E}-\mathbf{E}_h,\mathbf{E}-\mathbf{E}_h)| \\ &= |b_{\mathbf{E}}(\mathbf{E}-\mathbf{E}_h,\mathbf{E}-\Pi_{h,0}\mathbf{E})| \\ &\lesssim \|\mathbf{E}-\mathbf{E}_h\|_{curl}\|\mathbf{E}-\Pi_{h,0}\mathbf{E}\|_{curl}. \end{aligned}$$

Then, (33) follows from

$$\begin{aligned} \|\mathbf{E}-\Pi_{h,0}\mathbf{E}\|_{curl} &= |\mathcal{E}(\mathbf{J},\mathbf{M})-\Pi_{h,0}\mathcal{E}(\mathbf{J},\mathbf{M})|_0 + |\nabla\times(\mathcal{E}(\mathbf{J},\mathbf{M})-\Pi_{h,0}\mathcal{E}(\mathbf{J},\mathbf{M}))|_0 \\ &\lesssim \eta_h^{\mathbf{E}}\left(\|\mathbf{J}\|_{div}+|\mathbf{M}|_0\right)+\eta_h^{\mathbf{H}}\left(|\mathbf{J}|_0+\|\mathbf{M}\|_{curl}\right) \\ &\lesssim \left(\eta_h^{\mathbf{E}}+\eta_h^{\mathbf{H}}\right)\left(\|\mathbf{J}\|_{div}+\|\mathbf{M}\|_{curl}\right). \end{aligned}$$

□

As pointed out in [26], once the interpolation error estimates are established, Céa's lemma trivially implies the convergence of Nédélec's finite elements when the conductivity is strictly positive. In [26], Céa's Lemma is used exactly like in Theorem 6, with the notable difference that the conductivity σ is assumed to be continuous, and the solution $\mathbf{E}\in\mathbf{H}^2(\Omega)$. In this case, we immediately have $\eta_h^{\mathbf{E}}\simeq\eta_h^{\mathbf{H}}\simeq h$, so that Céa's Lemma directly yields optimal convergence rates, for both the electric and magnetic fields.

In [26], the author also considers the more difficult case where $\sigma=0$ and $\varepsilon>0$. Then, the sesquilinear form is no longer coercive, and special duality techniques have to be employed to prove the well-posedness and convergence in some asymptotic range. Then again, the solution is assumed to be regular, so that the final error estimate is linear in the full $H(curl)$-norm.

Generally speaking, when the solution is regular, it makes sense to measure finite element errors in the full $H(curl)$-norm, as its two components converge at the same rate: linearly. Also, in contrast with the Poisson problem, there is no need to use duality techniques *à la* Aubin-Nitsche, since the result given by Céa's lemma is already optimal.

In the case of heterogeneous media with discontinuous permittivity and permeability, both electrocmagnetic fields have low regularity, and it makes sense to derive error estimates in the full $H(curl)$-norm [27, 23] as well. The resulting convergence rate then corresponds to the lowest regularity of the two fields.

Here, since the magnetic field is always regular, we feel that it is important to distinguish the convergence rate of the two components of the $H(curl)$-norm, that is, the L^2-norm of the electric field, and the L^2-norm of the magnetic field. We first establish the electric field error estimate in Corollary 1. The magnetic field error estimate will be derived in Corollary 2 of the next subsection.

Since $\eta_h^{\mathbf{E}}+\eta_h^{\mathbf{H}}\simeq\eta_h^{\mathbf{E}}$, error estimate (33) is optimal for the electric field L^2-error. Indeed, it shows that the finite element solution converges as $\eta_h^{\mathbf{E}}$, just as the interpolant, in terms of the electric field L^2-error. We record this result in the next corollary, whose proof is a direct application of Theorems 5 and 6.

Corollary 1. *If $\mathcal{T}_h$ is a $\mathscr{P}$-fitting mesh, it holds that*

$$|\mathbf{E}-\mathbf{E}_h|_0 \lesssim h^s \left(\|\mathbf{J}\|_{div}+\|\mathbf{M}\|_{curl}\right), \tag{34}$$

for all $0<s<\tau(\sigma)$.

If $\tilde{\mathcal{T}}_h$ is a not $\mathscr{P}$-fitting, then only we have

$$|\mathbf{E}-\mathbf{E}_h|_0 \lesssim h^t \left(\|\mathbf{J}\|_{div}+\|\mathbf{M}\|_{curl}\right), \tag{35}$$

for all $0<t<\tilde{\tau}(\sigma)$.

2.3.3. *Magnetic field error estimates.* Corollary 1 provides an optimal error estimate for the electric field. However, if we apply directly Theorem 6 to estimate the magnetic field error in the L^2-norm, we obtain

$$|\nabla\times(\mathbf{E}-\mathbf{E}_h)|_0 \lesssim h^s \left(\|\mathbf{J}\|_{div}+\|\mathbf{M}\|_{curl}\right) \tag{36}$$

for all $0<s<\tau(\sigma)$ (or $\tilde{\tau}(\sigma)$ for a non-fitting mesh). However, from estimate (30) of Theorem 5, we know that the convergence rate of the interpolant is linear for the magnetic field in the sense that

$$|\nabla\times(\mathbf{E}-\Pi_{h,0}\mathbf{E})|_0 \lesssim h \left(\|\mathbf{J}\|_{div}+\|\mathbf{M}\|_{curl}\right).$$

As a result, it is unclear whether (36) is optimal. In the next theorem, we show that (36) is actually suboptimal and provide an improved error estimate for the magnetic field.

Theorem 7. *It holds that*

$$|\nabla\times(\mathbf{E}-\mathbf{E}_h)|_0 \lesssim \left(\eta_h^{\mathbf{H}}+(\eta_h^{\mathbf{E}}+\eta_h^{\mathbf{H}})^2\right)\left(\|\mathbf{J}\|_{div}+\|\mathbf{M}\|_{curl}\right). \tag{37}$$

Proof. The proof relies on the Aubin-Nitsche duality trick, which needs to be slightly modified for our purpose. We define $\boldsymbol{\phi}\in\mathbf{H}_0(curl,\Omega)$ as the unique solution of

$$b_{\mathbf{E}}(\mathbf{v},\boldsymbol{\phi}) = (\nabla\times\mathbf{v},\nabla\times(\mathbf{E}-\mathbf{E}_h)), \quad \forall\mathbf{v}\in\mathbf{H}_0(curl,\Omega). \tag{38}$$

It can be easily seen that $\boldsymbol{\phi}=\overline{\mathcal{E}(\mathbf{j},\mathbf{m})}$ with $\mathbf{j}=\mathbf{0}$ and $\mathbf{m}=\overline{\nabla\times(\mathbf{E}-\mathbf{E}_h)}$. Because $\mathbf{0}=\mathbf{j}\in\mathbf{H}(div,\Omega)$, we have

$$|\boldsymbol{\phi}-\Pi_{h,0}\boldsymbol{\phi}|_0 \le \eta_h^{\mathbf{E}}|\mathbf{m}|_0 = \eta_h^{\mathbf{E}}|\nabla\times(\mathbf{E}-\mathbf{E}_h)|_0. \tag{39}$$

Since $\nabla\times\mathbf{E}_h$ is a discontinuous (piecewise constant) function, $\mathbf{m}\notin\mathbf{H}(curl,\Omega)$ and we can not bound $|\nabla\times(\boldsymbol{\phi}-\Pi_{h,0}\boldsymbol{\phi})|_0$ directly. Hence, we introduce a decomposition of $\boldsymbol{\phi}$ as $\boldsymbol{\phi}=\mathbf{E}-\mathbf{E}_h+\boldsymbol{\psi}$, with $\boldsymbol{\psi}\in\mathbf{H}_0(curl,\Omega)$ (because $\mathbf{E},\mathbf{E}_h\in\mathbf{H}_0(curl,\Omega)$) solution of

$$b_{\mathbf{E}}(\mathbf{v},\boldsymbol{\psi}) = b_{\mathbf{E}}(\mathbf{v},\boldsymbol{\phi})-b_{\mathbf{E}}(\mathbf{v},\mathbf{E}-\mathbf{E}_h) = (\mathbf{v},-\sigma(\mathbf{E}-\mathbf{E}_h)), \forall\mathbf{v}\in\mathbf{H}_0(curl,\Omega).$$

This equivalently means that $\boldsymbol{\psi}=\overline{\mathcal{E}(\mathbf{j},\mathbf{m})}$ with $\mathbf{j}=-\sigma\overline{(\mathbf{E}-\mathbf{E}_h)}$ and $\mathbf{m}=\mathbf{0}$. Then, we have $\mathbf{0}=\mathbf{m}\in\mathbf{H}(curl,\Omega)$ and it follows that

$$\begin{aligned}
|\nabla\times(\boldsymbol{\phi}-\Pi_{h,0}\boldsymbol{\phi})|_0 &\le |\nabla\times((\mathbf{E}-\mathbf{E}_h)-\Pi_{h,0}(\mathbf{E}-\mathbf{E}_h))|_0+|\nabla\times(\boldsymbol{\psi}-\Pi_{h,0}\boldsymbol{\psi})|_0\\
&\lesssim |\nabla\times(\mathbf{E}-\Pi_{h,0}\mathbf{E})|_0+\eta_h^{\mathbf{H}}|\sigma(\mathbf{E}-\mathbf{E}_h)|_0\\
&\lesssim |\nabla\times(\mathbf{E}-\Pi_{h,0}\mathbf{E})|_0+\eta_h^{\mathbf{H}}|(\mathbf{E}-\mathbf{E}_h)|_0.
\end{aligned}$$

By definition of $\boldsymbol{\phi}$ and by Galerkin orthogonality, we have

$$\begin{aligned}
|\nabla\times(\mathbf{E}-\mathbf{E}_h)|_0^2 &= b_{\mathbf{E}}(\mathbf{E}-\mathbf{E}_h,\boldsymbol{\phi})\\
&= b_{\mathbf{E}}(\mathbf{E}-\mathbf{E}_h,\boldsymbol{\phi}-\Pi_{h,0}\boldsymbol{\phi})\\
&\lesssim |\mathbf{E}-\mathbf{E}_h|_0|\boldsymbol{\phi}-\Pi_{h,0}\boldsymbol{\phi}|_0+|\nabla\times(\mathbf{E}-\mathbf{E}_h)|_0|\nabla\times(\boldsymbol{\phi}-\Pi_{h,0}\boldsymbol{\phi})|_0\\
&\lesssim \eta_h^{\mathbf{E}}|\mathbf{E}-\mathbf{E}_h|_0|\nabla\times(\mathbf{E}-\mathbf{E}_h)|_0+|\nabla\times(\mathbf{E}-\mathbf{E}_h)|_0|\nabla\times(\boldsymbol{\phi}-\Pi_{h,0}\boldsymbol{\phi})|_0.
\end{aligned}$$

Simplifying by $|\nabla\times(\mathbf{E}-\mathbf{E}_h)|_0$, we conclude that

$$\begin{aligned}
|\nabla\times(\mathbf{E}-\mathbf{E}_h)|_0 &\lesssim \eta_h^{\mathbf{E}}|\mathbf{E}-\mathbf{E}_h|_0+|\nabla\times(\boldsymbol{\phi}-\Pi_{h,0}\boldsymbol{\phi})|_0\\
&\lesssim |\nabla\times(\mathbf{E}-\Pi_{h,0}\mathbf{E})|_0+(\eta_h^{\mathbf{E}}+\eta_h^{\mathbf{H}})|\mathbf{E}-\mathbf{E}_h|_0,
\end{aligned}$$

and (37) follows since, from Theorems 5 and 6, we have

$$|\nabla\times(\mathbf{E}-\Pi_{h,0}\mathbf{E})|_0\lesssim\eta_h^{\mathbf{H}}\left(\|\mathbf{J}\|_{div}+\|\mathbf{M}\|_{curl}\right),$$

and

$$|\mathbf{E}-\mathbf{E}_h|_0\lesssim(\eta_h^{\mathbf{E}}+\eta_h^{\mathbf{H}})\left(\|\mathbf{J}\|_{div}+\|\mathbf{M}\|_{curl}\right).$$

□

In Corollary 2, we directly apply Theorem 7 to provide explicit convergence rates in terms of mesh size, for both fitting and non-fitting meshes. We see that fitting and non-fitting meshes deliver virtually the same convergence rates (up to an arbitrarily small constant δ).

Corollary 2. *Assume that $\tau(\sigma)\leq 1/2$. Then it holds*

$$|\nabla\times(\mathbf{E}-\mathbf{E}_h)|_0\lesssim h^{2s}\left(\|\mathbf{J}\|_{div}+\|\mathbf{M}\|_{curl}\right), \tag{40}$$

for all $0<s<\tau(\sigma)$ for both fitting and non-fitting meshes.

If $\tau(\sigma)>1/2$, then we have

$$|\nabla\times(\mathbf{E}-\mathbf{E}_h)|_0\lesssim h\left(\|\mathbf{J}\|_{div}+\|\mathbf{M}\|_{curl}\right), \tag{41}$$

for fitting meshes and

$$|\nabla\times(\mathbf{E}-\mathbf{E}_h)|_0\lesssim h^{1-\delta}\left(\|\mathbf{J}\|_{div}+\|\mathbf{M}\|_{curl}\right), \tag{42}$$

for non-fitting meshes.

Proof. The proof simply relies on a careful inspection of the factor $\eta_h^{\mathbf{H}}+(\eta_h^{\mathbf{E}}+\eta_h^{\mathbf{H}})^2$ in (37). Recalling Theorem 5, we have $\eta_h^{\mathbf{H}}\lesssim h$ and $\eta_h^{\mathbf{E}}\lesssim h^t$ for all $0<t<\theta$, where $\theta=\tau(\sigma)$ or $\tilde{\tau}(\sigma)$. Then, we obtain

$$\begin{aligned}
\eta_h^{\mathbf{H}}+(\eta_h^{\mathbf{E}}+\eta_h^{\mathbf{H}})^2 &\lesssim \eta_h^{\mathbf{H}}(1+\eta_h^{\mathbf{H}}+\eta_h^{\mathbf{E}})+(\eta_h^{\mathbf{E}})^2\\
&\lesssim \eta_h^{\mathbf{H}}+(\eta_h^{\mathbf{E}})^2\\
&\lesssim \max(\eta_h^{\mathbf{H}},(\eta_h^{\mathbf{E}})^2)\\
&\lesssim \max(h,h^{2t})\\
&\lesssim h^{\min(1,2t)},
\end{aligned} \tag{43}$$

for all $0<t<\theta$. If $\tau(\sigma)\leq 1/2$, then $\theta=\tau(\sigma)=\tilde{\tau}(\sigma)$ and (40) follows from (43).

When $\mathcal{T}_h$ is a fitting mesh and $\tau(\sigma) > 1/2$, we have $\min(1, 2t) = 1$, so that (41) follows from (43).

Now, if $\tilde{\mathcal{T}}_h$ is a non-fitting mesh and $\tau(\sigma) > 1/2$, then $\tilde{\tau}(\sigma) = 1/2$. It follows that there exists a $t \in (0, \tilde{\tau}(\sigma))$ such that $t > (1-\delta)/2$, and then we have $\min(1, 2t) = 1 - \delta$, so that (42) follows from (43). □

2.4. **The magnetic field formulation.** We now consider the discretization of the magnetic field formulation (5) using Nédélec's edge elements. The discrete magnetic field is sought as the element $\mathbf{H}_h \in \mathbf{V}_h$ satisfying

$$b_{\mathbf{H}}(\mathbf{H}_h, \mathbf{v}_h) = (\mathbf{M}, \mathbf{v}_h) + (\sigma^{-1}\mathbf{J}, \nabla \times \mathbf{v}_h), \quad \forall \mathbf{v}_h \in \mathbf{V}_h. \tag{44}$$

The discrete electric field is approximated as $\mathbf{E}_h = \sigma^{-1}(\mathbf{J} - \nabla \times \mathbf{H}_h)$. Following the electric case, the quantity $|\nabla \times (\mathbf{H} - \mathbf{H}_h)|_0$ will be referred to as "electric field" error, while we will denote $|\mathbf{H} - \mathbf{H}_h|_0$ as the "magnetic field" error.

Our analysis will be analogous to that of the electric field formulation, and we shall provide fewer details. In particular, the proofs of Theorems 8 and 9 as well as Corollaries 3 and 4 are omitted, because they are analogous to their E-formulation counterparts.

As for the electric field formulation, we require some regularity on the right-hand-sides. Following Theorem 4, we assume that $\sigma^{-1}\mathbf{J} \in \mathbf{H}_0(curl, \Omega)$ and $\mathbf{M} \in \mathbf{H}_0(div, \Omega)$. We remark that the regularity assumptions are different than in the electric field formulation. Though we do not investigate numerically this aspect in this work, it might be useful to select between the **E** and **H**-formulations depending on the type of electromagnetic sources in presence.

2.4.1. *Interpolation error estimates.* For $\mathbf{j}, \mathbf{m} \in \mathbf{L}^2(\Omega)$, let $\mathcal{H}(\mathbf{j}, \mathbf{m})$ be the unique element $\mathcal{H}(\mathbf{j}, \mathbf{m}) \in \mathbf{H}(curl, \Omega)$ such that

$$b_{\mathbf{H}}(\mathcal{H}(\mathbf{j}, \mathbf{m}), \mathbf{v}) = (\mathbf{m}, \mathbf{v}) + (\sigma^{-1}\mathbf{j}, \nabla \times \mathbf{v}), \quad \forall \mathbf{v} \in \mathbf{H}(curl, \Omega).$$

We define

$$\eta_h^{\mathbf{E}} = \sup_{\sigma^{-1}\mathbf{j} \in \mathbf{H}_0(curl,\Omega), \mathbf{m} \in \mathbf{L}^2(\Omega)} \frac{|\nabla \times (\mathcal{H}(\mathbf{j}, \mathbf{m}) - \Pi_h \mathcal{H}(\mathbf{j}, \mathbf{m}))|_0}{\|\sigma^{-1}\mathbf{j}\|_{curl} + |\mathbf{m}|_0},$$

and

$$\eta_h^{\mathbf{H}} = \sup_{\mathbf{j} \in \mathbf{L}^2(\Omega), \mathbf{m} \in \mathbf{H}_0(div,\Omega)} \frac{|\mathcal{H}(\mathbf{j}, \mathbf{m}) - \Pi_h \mathcal{H}(\mathbf{j}, \mathbf{m})|_0}{|\mathbf{j}|_0 + \|\mathbf{m}\|_{div}},$$

which characterize the approximation properties of the interpolant.

Theorem 8. *It holds that*

$$\eta_h^{\mathbf{H}} \lesssim h, \tag{45}$$

for both $\mathscr{P}$-fitting and non $\mathscr{P}$-fitting meshes.

If $\mathcal{T}_h$ is a $\mathscr{P}$-fitting mesh, we have

$$\eta_h^{\mathbf{E}} \lesssim h^s, \tag{46}$$

for all $0 < s < \tau(\sigma)$.

If $\tilde{\mathcal{T}}_h$ is not a $\mathscr{P}$-fitting mesh, then we only have

$$\eta_h^{\mathbf{E}} \lesssim h^t, \tag{47}$$

for all $0 < t < \tilde{\tau}(\sigma)$.

2.4.2. *Electric field error estimate.* In the following theorem, we apply Céa's lemma to prove the convergence of the finite element solution.

Theorem 9. *There exists a unique $\mathbf{H}_h \in \mathbf{V}_h$ satisfying (44). Furthermore, we have*

$$\|\mathbf{H} - \mathbf{H}_h\|_{curl} \lesssim \left(\eta_h^{\mathbf{H}} + \eta_h^{\mathbf{E}}\right)\left(\|\sigma^{-1}\mathbf{J}\|_{curl} + \|\mathbf{M}\|_{div}\right). \tag{48}$$

As in the electric field formulation, the above result is optimal in terms of the electric field approximation. We record this result in Corollary 3.

Corollary 3. *If $\mathcal{T}_h$ is a $\mathscr{P}$-fitting mesh, it holds that*

$$|\nabla \times (\mathbf{H} - \mathbf{H}_h)|_0 \lesssim h^s \left(\|\sigma^{-1}\mathbf{J}\|_{curl} + \|\mathbf{M}\|_{div}\right), \tag{49}$$

for all $0 < s < \tau(\sigma)$.

If $\tilde{\mathcal{T}}_h$ is a not $\mathscr{P}$-fitting, then we have

$$|\nabla \times (\mathbf{H} - \mathbf{H}_h)|_0 \lesssim h^t \left(\|\sigma^{-1}\mathbf{J}\|_{curl} + \|\mathbf{M}\|_{div}\right), \tag{50}$$

for all $0 < t < \tilde{\tau}(\sigma)$.

2.4.3. *Magnetic field error estimates.* As in the electric field formulation, our key result is an improved convergence rate for the magnetic field L^2-error.

Theorem 10. *It holds that*

$$|\mathbf{H} - \mathbf{H}_h|_0 \lesssim \left(\eta_h^{\mathbf{H}} + \left(\eta_h^{\mathbf{E}} + \eta_h^{\mathbf{H}} + h\right)\left(\eta_h^{\mathbf{E}} + \eta_h^{\mathbf{H}}\right)\right)\left(\|\sigma^{-1}\mathbf{J}\|_{curl} + \|\mathbf{M}\|_{div}\right). \tag{51}$$

Proof. The proof is again based on a modified version of the Aubin-Nitsche duality argument. We first introduce the Hodge-Helmholtz decomposition of the error vector:

$$\mathbf{H} - \mathbf{H}_h = \nabla p + \boldsymbol{\phi},$$

with $p \in H^1(\Omega)$, $\boldsymbol{\phi} \in \mathbf{H}(curl, \Omega)$, $\nabla \cdot \boldsymbol{\phi} = 0$ and $\boldsymbol{\phi} \cdot \mathbf{n} = 0$. Then, we have

$$\Pi_h \mathbf{H} - \mathbf{H}_h = \Pi_h(\mathbf{H} - \mathbf{H}_h) = \nabla r^h(p) + \Pi_h \boldsymbol{\phi}.$$

Hence it remains to bound $|\nabla p|_0$ and $|\boldsymbol{\phi}|_0$. To this end, we introduce $\boldsymbol{\psi} = \overline{\mathcal{H}(\mathbf{j}, \mathbf{m})}$, with $\mathbf{j} = \mathbf{0}$ and $\mathbf{m} = \overline{\boldsymbol{\phi}}$ so that, by Galerkin orthogonality

$$|\boldsymbol{\phi}|_0^2 = (\mathbf{H} - \mathbf{H}_h, \boldsymbol{\psi}) = b_{\mathbf{H}}(\mathbf{H} - \mathbf{H}_h, \boldsymbol{\psi}) = b_{\mathbf{H}}(\mathbf{H} - \mathbf{H}_h, \boldsymbol{\psi} - \Pi_h \boldsymbol{\psi}).$$

Since $\mathbf{0} = \mathbf{j} \in \mathbf{H}_0(curl, \Omega)$, and because $\nabla \cdot \boldsymbol{\phi} = 0$ and $\boldsymbol{\phi} \cdot \mathbf{n} = 0$, we have $\mathbf{m} = \overline{\boldsymbol{\phi}} \in \mathbf{H}_0(div, \Omega)$ and $\|\mathbf{m}\|_{div} = |\boldsymbol{\phi}|_0$. As a result, we obtain

$$\begin{aligned} |b_{\mathbf{H}}(\mathbf{H} - \mathbf{H}_h, \boldsymbol{\psi} - \Pi_h \boldsymbol{\psi})| &\lesssim \eta_h^{\mathbf{H}} |\mathbf{H} - \mathbf{H}_h|_0 |\boldsymbol{\psi} - \Pi_h \boldsymbol{\psi}|_0 + \eta_h^{\mathbf{E}} |\nabla \times (\mathbf{H} - \mathbf{H}_h)|_0 |\nabla \times (\boldsymbol{\psi} - \Pi_h \boldsymbol{\psi})|_0, \\ &\lesssim \eta_h^{\mathbf{H}} |\mathbf{H} - \mathbf{H}_h|_0 |\boldsymbol{\phi}|_0 + \eta_h^{\mathbf{E}} |\nabla \times (\mathbf{H} - \mathbf{H}_h)|_0 |\boldsymbol{\phi}|_0, \end{aligned}$$

so that

$$|\boldsymbol{\phi}|_0 \lesssim \eta_h^{\mathbf{H}} |\mathbf{H} - \mathbf{H}_h|_0 + \eta_h^{\mathbf{E}} |\nabla \times (\mathbf{H} - \mathbf{H}_h)|_0.$$

Using Theorem 9, we obtain

$$|\boldsymbol{\phi}|_0 \lesssim (\eta_h^{\mathbf{H}} + \eta_h^{\mathbf{E}})^2 \left(\|\mathbf{J}\|_{curl} + \|\mathbf{M}\|_{div}\right). \tag{52}$$

For the estimate of $|\nabla p|_0$, first as $(\boldsymbol{\phi}, \nabla p) = 0$, we can write

$$\begin{aligned} |\nabla p|_0^2 &= (\mathbf{H} - \mathbf{H}_h, \nabla p) \\ &= (\Pi_h \mathbf{H} - \mathbf{H}_h, \nabla p) + (\mathbf{H} - \Pi_h \mathbf{H}, \nabla p) \\ &= (\nabla r^h(p) + \Pi_h \boldsymbol{\phi}, \nabla p) + (\mathbf{H} - \Pi_h \mathbf{H}, \nabla p). \\ &= (\nabla r^h(p), \nabla p) + (\Pi_h \boldsymbol{\phi} - \boldsymbol{\phi}, \nabla p) + (\mathbf{H} - \Pi_h \mathbf{H}, \nabla p). \end{aligned}$$

Now, we observe that, if $q^h \in S^h$, then $\nabla \times \nabla q^h = \mathbf{0}$, and we have

$$(\nabla p, \nabla q^h) = (\mathbf{H} - \mathbf{H}_h, \nabla q^h) = b_{\mathbf{H}}(\mathbf{H} - \mathbf{H}_h, \nabla q^h) = 0.$$

In particular, $(\nabla r^h(p), \nabla p) = 0$, and we have

$$|\nabla p|_0^2 = (\Pi_h \boldsymbol{\phi} - \boldsymbol{\phi}, \nabla p) + (\mathbf{H} - \Pi_h \mathbf{H}, \nabla p),$$

so that

$$|\nabla p|_0 \leq |\boldsymbol{\phi} - \Pi_h \boldsymbol{\phi}|_0 + |\mathbf{H} - \Pi_h \mathbf{H}|_0.$$

Since $\nabla \cdot \boldsymbol{\phi} = 0$ and $\boldsymbol{\phi} \cdot \mathbf{n} = 0$, we have (see [19], Theorem I.3.9) $\boldsymbol{\phi} \in \mathbf{H}^1(\Omega)$ and $|\boldsymbol{\phi}|_1 \lesssim |\nabla \times \boldsymbol{\phi}|_0$. Then,

$$|\boldsymbol{\phi} - \Pi_h \boldsymbol{\phi}|_0 \lesssim h|\boldsymbol{\phi}|_1 \lesssim h|\nabla \times \boldsymbol{\phi}|_0 = h|\nabla \times (\mathbf{H} - \mathbf{H}_h)|_0.$$

As a result, we obtain

$$|\nabla p|_0 \lesssim h|\nabla \times (\mathbf{H} - \mathbf{H}_h)|_0 + |\mathbf{H} - \Pi_h \mathbf{H}|_0 \lesssim h(\eta_h^{\mathbf{E}} + \eta_h^{\mathbf{H}}) + \eta_h^{\mathbf{H}} \tag{53}$$

Error estimate (51) then follows from (52) and (53). □

Like in the electric field formulation, Corollary 4 provides optimal convergence rates in the general case.

Corollary 4. *Assume that $\tau(\sigma) \leq 1/2$. Then it holds*

$$|\mathbf{H} - \mathbf{H}_h|_0 \lesssim h^{2s} \left(\|\sigma^{-1}\mathbf{J}\|_{curl} + \|\mathbf{M}\|_{div}\right), \tag{54}$$

for all $0 < s < \tau(\sigma)$ for both fitting and non-fitting meshes.
If $\tau(\sigma) > 1/2$, then we have

$$|\mathbf{H} - \mathbf{H}_h|_0 \lesssim h \left(\|\sigma^{-1}\mathbf{J}\|_{curl} + \|\mathbf{M}\|_{div}\right), \tag{55}$$

for fitting meshes and

$$|\mathbf{H} - \mathbf{H}_h|_0 \lesssim h^{1-\delta} \left(\|\sigma^{-1}\mathbf{J}\|_{curl} + \|\mathbf{M}\|_{div}\right), \tag{56}$$

for non-fitting meshes.

3. Numerical experiments

3.1. **Settings.** In this section, we describe the 2D numerical experiments we have selected to illustrate our error estimates proved in the previous section. For the sake of simplicity, we consider as computational domain the unit square $\Omega = (0,1)^2$.

The target applications for the proposed method are borehole logging simulations. For this type of applications, the domain is the whole space, but it is artificially bounded for numerical computations. Since sources are localized, the electromagnetic fields exhibit an exponential decay as a function of the distance from the source, and truncating the domain only introduces a small modelization error. The choice of the domain size is guided by the so-called "skin-depth relation", which links the frequency, the conductivity, and the decay rate of the electromagnetic fields. We refer the reader to [36].

The value of the conductivity ranges from $10^{-3}\mathrm{Sm}^{-1}$ to $5\mathrm{Sm}^{-1}$ in our numerical experiments. Hence, based on the skin-depth relation, we select the frequency $f = 2$ Mhz (and $\omega = 2\pi f$). In this way, the frequency, the domain size, and the conductivity model are representative of borehole logging applications.

Fitting and non-fitting meshes are considered in the following numerical experiments. When a non-fitting mesh is used, the "exact quadrature method" [11, 6] is used to integrate the coefficients of the finite element linear system exactly.

3.1.1. *Meshes and finite element spaces.* We use cartesian grid based meshes with square cells. Hence, given $h = 1/n$, the mesh $\mathcal{T}_h$ is defined as

$$\mathcal{T}_h = \{K = ((i-1)h, ih) \times ((j-1)h, jh), \quad 1 \leq i, j \leq n\}.$$

Because meshes $\mathcal{T}_h$ are made of squares, we need to slightly modify the definitions of the Nédélec's element spaces given in Section 2. Hence, we introduce

$$\mathbf{V}_h = \{\mathbf{v}_h \in \mathbf{H}(curl, \Omega) \quad | \quad \mathbf{v}_h|_K \in \nabla Q_1(K), \quad \forall K \in \mathcal{T}_h\}$$

where $Q_1(K) = \mathrm{span}\{1, x, z, xz\}$. We also define $\mathbf{V}_{h,0} = \mathbf{V}_h \cap H_0(curl, \Omega)$.

3.1.2. *Error computations.* In order to compute numerical errors, we will use a finite element solution computed on a fine mesh. In our convergence curves, the values of n range from 512 to 2048. We select $n = 4096$ to compute the reference finite element solution.

Also, an important part of our analysis stays on the comparison between fitting and non-fitting meshes. In order to carry out such comparison, we select a piecewise constant conductivity σ that is discontinuous only at the interfaces $\Gamma_h = (0,1) \times \{0.5\}$ and $\Gamma_v = \{0.5\} \times (0,1)$. Then, it is easily seen that if n is an even integer, both Γ_h and Γ_v are covered by mesh edges, so that the mesh is fitting. On the other hand, if n is an odd integer, the two interfaces lie in the interior of some mesh cells, leading to a non-fitting mesh. Thus, when comparing fitting and non-fitting meshes, we will compare meshes with an even number of subdivisions n with meshes having an odd number of subdivisions. We refer the reader to Figure 2, where the difference between fitting and non-fitting meshes is highlighted.

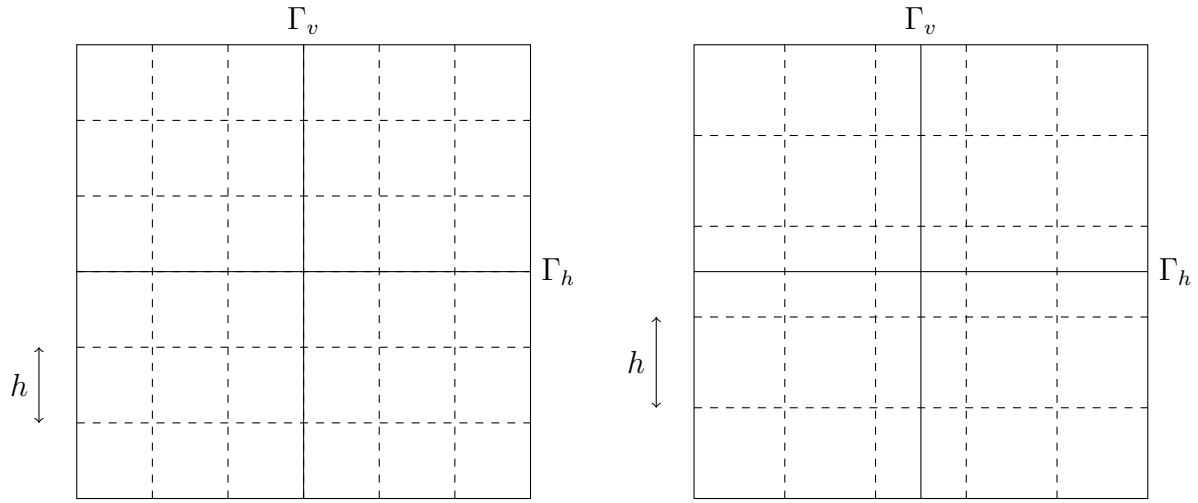

(a) Fitting mesh ($n = 6$) (b) Non-fitting mesh ($n = 5$)

FIGURE 2. Fitting and Non-fitting meshes

3.2. **Validation experiments.** We first present two validation experiments. For both experiments, the conductivity parameter is given by

$$\sigma(x,z) = \begin{cases} 1 & \text{if } x < 0.5, z > 0.5 \\ \sigma_b & \text{if } x > 0.5, z > 0.5 \\ \sigma_b & \text{if } x < 0.5, z < 0.5 \\ 1 & \text{if } x > 0.5, z < 0.5, \end{cases}$$

where σ_b is a chosen constant, and we use the right-hand-side $\mathbf{J} = (1, 0, 1)$.

Since we are in a 2D setting, singularities do not occur in the TE polarization; hence we focus on the TM-polarization. For this polarization, we have $\mathbf{E} = (E_x, 0, E_z)$ and $\mathbf{H} = (0, H_y, 0)$, furthermore an analytical expression of $\tau(\sigma)$ is available from [15]. Then, we discretize the problem using formulation (28) for (E_x, E_z) and compute an approximation of H_y by post-processing (compare with (29))

$$H_{y,h} = \mathbf{H}_h = \frac{1}{i\omega\mu_0} \operatorname{curl} (E_{x,h}, E_{z,h}),$$

where $(E_{x,h}, E_{z,h})$ is the unique solution of (28).

For this choice of conductivity parameter, we have an analytical expression for the regularity coefficient of the electric field. Based on Theorem 8.1 of [15], the expected regularity of the solution is $\mathbf{E} \in \mathbf{H}^{\tau(\sigma)}(\Omega)$, where

$$\tau(\sigma) = \frac{4}{\pi} \arctan\left(\sqrt{\sigma_b}\right). \tag{57}$$

Here, we measure the global L^2 error norm, i.e.,

$$e_\Omega(\phi) = \frac{|\phi - \phi_h|_0}{|\phi|_0}, \quad \phi = \mathbf{E}, H_y.$$

3.2.1. *Experiment A.* We first consider the case where $\tau(\sigma) > 1/2$. Hence, we select the value $\sigma_b = 0.5$, so that (57) yields $\tau(\sigma) \simeq 0.78$.

As seen on Figure 3, we observe a convergence rate in $\mathcal{O}(h^{\tau(\sigma)})$ for the electric field approximation when using fitting meshes.

We also observe on Figure 3 that when non-fitting meshes are used, the electric field approximation converges only as $\mathcal{O}(h^{1/2})$. This is in accordance with our analysis. Indeed, since $\tau(\sigma) > 1/2$, we have $\tilde{\tau}(\sigma) = 1/2$.

Finally, Figure 3 shows that the convergence for the magnetic field is in $\mathcal{O}(h)$ for both fitting and non-fitting meshes, as expected.

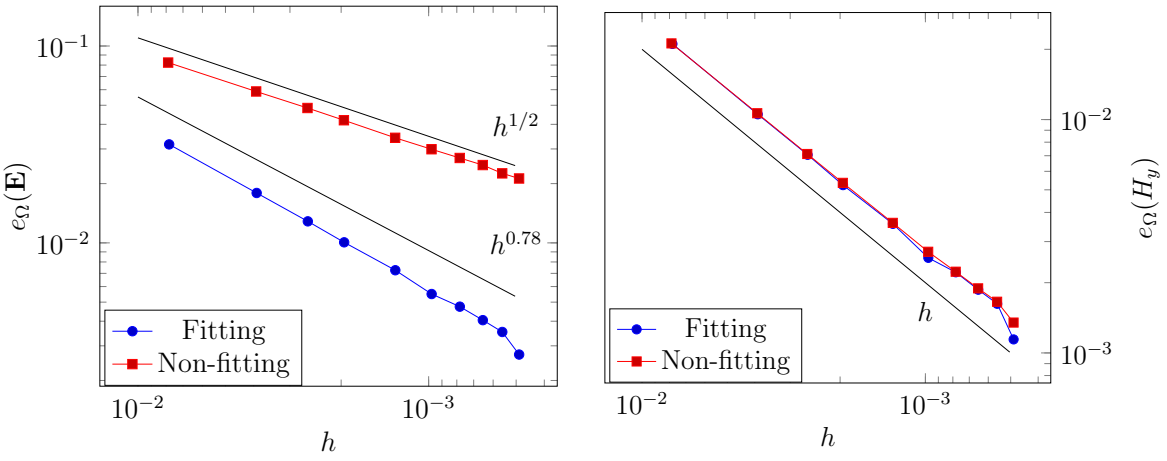

(a) Electric field errors

(b) Magnetic field errors

FIGURE 3. Experiment A

3.2.2. *Experiment B.* We now consider the case $\tau(\sigma) < 1/2$. We set $\sigma_b = 0.1$, so that $\tau(\sigma) \simeq 0.39$.

As Figure 4 shows, non-fitting meshes exhibit the expected results exactly. Indeed, the convergence rate for the electric field is $\tilde{\tau}(\sigma) = \tau(\sigma) \simeq 0.39$, and the magnetic field converges as $2\tilde{\tau}(\sigma)$.

Figure 4 presents the results obtained with fitting meshes. As shown there, both the electric and magnetic approximations converge faster than expected, at rates 1/2 and 1 respectively.

These results are rather surprising since we observe that the electric field approximation converges faster than $\tau(\sigma)$, which is the convergence rate of the best approximation. This is not in contradiction with our theoretical analysis, since we only show upper bounds. However, these results question the optimality of the presented analysis.

The authors believe, however, that the proposed error-estimates are optimal, and that the observed super-convergence rate can be explained by a pre-asymptotic effect. Indeed, we can decompose $\mathbf{E}$ as

$$\mathbf{E} = \mathbf{E}_s + \mathbf{E}_r,$$

where $\mathbf{E}_s \in \mathbf{H}^{\tau(\sigma)}(\Omega)$ and $\mathbf{E}_r \in \mathbf{H}^1(\Omega)$ correspond to singular and regular parts of the electric field. Consequently, if $\|\mathbf{E}\|_{s,\Omega} \lll \|\mathbf{E}_r\|_{1,\Omega}$, it is reasonable to expect a super-convergence phenomena as far as the mesh sizes h are relatively coarse.

Additionally, we show in subsection 3.3.3 another test with a singular solution for which the predicted behaviour is observed for both fitting and non-fitting meshes.

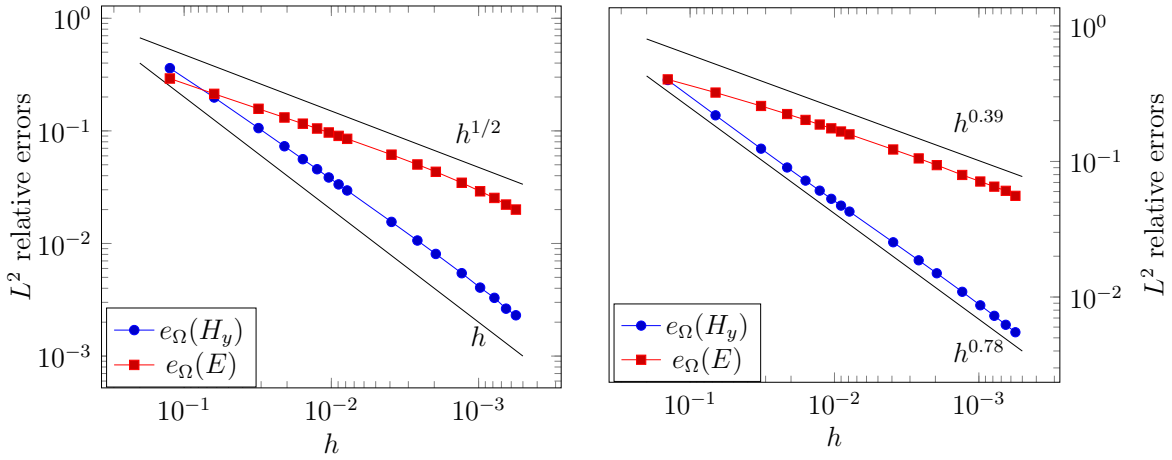

(a) Fitting meshes

(b) Non-fitting meshes

FIGURE 4. Experiment B

3.3. **"Geophysical" experiments.** We provide another set of numerical experiments directed toward geophysical applications. The sources are Gaussian loads representing electric transmitters. The L^2 error is measured locally in a small area representing a magnetic or electric receiver.

3.3.1. *Experiment 1.* We start with a test case using the TE-polarization. We consider a conductivity model featuring two layers, separated by a planar interface. In the top layer, the conductivity takes the value 1 Sm^{-1}. In the bottom layer, we consider three different tests with different values $\sigma_b \in \{0.9, 0.1, 0.001\}$ Sm^{-1} of σ. In that way, we are able to analyse the influence of the conductivity contrast.

The interface is located at depth $z = 0.5$m. Hence, the conductivity is defined as

$$\sigma(x,z) = \begin{cases} 1 \quad \mathrm{Sm}^{-1} & \text{if } z > 0.5 \\ \sigma_b \quad \mathrm{Sm}^{-1} & \text{if } z < 0.5. \end{cases}$$

We consider the source $\mathbf{J} = (0, g, 0)$ where g is a Gaussian load centered at $(0.4, 0.4)$:

$$g(x, z) = \exp\left(-\frac{(x-0.4)^2 + (z-0.4)^2}{(10^{-2})^2}\right).$$

The electric field has only one non-zero component ($\mathbf{E} = (0, E_y, 0)$), and the magnetic field takes the form $\mathbf{H} = (H_x, 0, H_z)$. Because the electric field has only one non-zero component, the electric field formulation employs Lagrange H^1-conforming elements. Since in this work we are mostly interested in Nédélec's elements, we will therefore focus on the magnetic field formulation. In other words, we approximate (H_x, H_z) by using (44) and compute a discrete electric field approximation as $E_{y,h} = \sigma^{-1}(g - \text{ curl } (H_{x,h}, H_{z,h}))$.

We measure the L^2 error in a subdomain $R = (0.6, 0.8) \times (0.6, 0.8)$ located "far" from the source center, in the bottom layer. Hence, we will measure the approximation errors as

$$e_R(\phi) = \frac{|\phi - \phi_h|_{0,R}}{|\phi|_{0,R}}, \quad \phi = E_y, H_x, H_z.$$

Physically, the quantity $\phi|_R$ ($\phi = E_y, H_x, H_z$) can be understood as the measure of electromagnetic fields at a receiver location. Thus, the quantities $e_R(\phi)$ are actually a good indicator of the error on the quantity of interest in borehole applications.

Figure 5 shows the results of Experiment 1. The predicted converge rates are observed. Indeed, we have $e_R(H_x) \lesssim h$, $e_R(H_y) \lesssim h$, and $e_R(E_y) \lesssim h^{1/2}$.

The case of a "small" contrast is represented by $\sigma_b = 0.9$ at Figure 5 (a). In this case, we observe similar results for fitting and non-fitting meshes, although some discrepancies are observed for the $e_R(E_y)$ case. Furthermore, we see that for non-fitting meshes, the convergence of the electric field is quasi linear in some pre-asymptotic range, and decreases asymptotically for small h.

In Figures 5 (b) and (c), higher contrasts are considered. In these cases, the convergence rate of the electric field clearly decreases for non-fitting meshes, and we observe the predicted convergence rate $\mathcal{O}(h^{1/2})$. For the magnetic field, the predicted convergence rate is respected, as the convergence is linear, both for fitting and non-fitting meshes. We see that the magnetic field error is greater by a constant factor for non-fitting meshes. Nonetheless, this factor is rather small, and increases reasonably slowly with the conductivity contrast. Indeed, even for the highest contrast (1 to $\sigma_b = 10^{-3}$) the accuracy loss due to the use of non-fitting meshes is limited to a factor of two.

3.3.2. *Experiment 2.* We now consider an experiment in the TM-polarization. We keep the same settings as Experiment 1, except that the source now reads

$$\mathbf{J} = (0, 0, g),$$

with the same Gaussian g as before. The magnetic field has only one non-zero component H_y and we have $\mathbf{E} = (E_x, 0, E_z)$. We will therefore focus on the electric field formulation (28).

Results are presented in Figure 6. The conclusions are similar those obtained for the case of TE-polarization presented in Experiment 1. First, we observe that the convergence

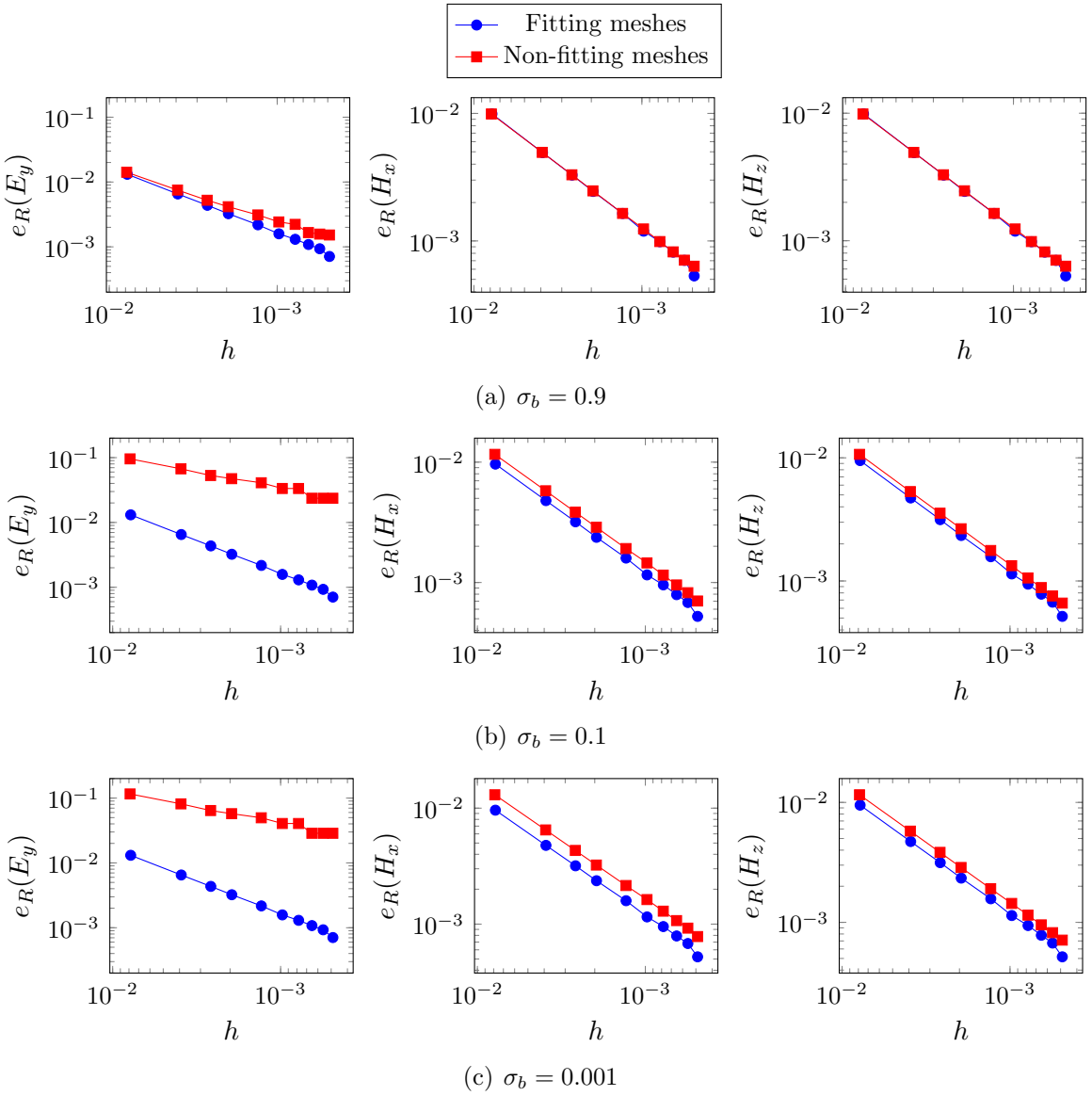

(a) $\sigma_b = 0.9$

(b) $\sigma_b = 0.1$

(c) $\sigma_b = 0.001$

FIGURE 5. Experiment 1

rates predicted by the theoretical analysis are strictly respected. The magnetic field approximation convergence is linear for fitting and non-fitting meshes and the electric field convergence rate is at worst $1/2$.

Again, we see that for a small conductivity contrast, the electric field approximation with non-fitting meshes has quasi-linear convergence in a pre-asymptotic range, and deteriorates as h goes to zero. Also, concerning the magnetic field, the non-fitting mesh error is higher than the fitting mesh error by a constant factor that grows with the conductivity contrast. Nevertheless, this constant remains small, even for the highest considered contrast.

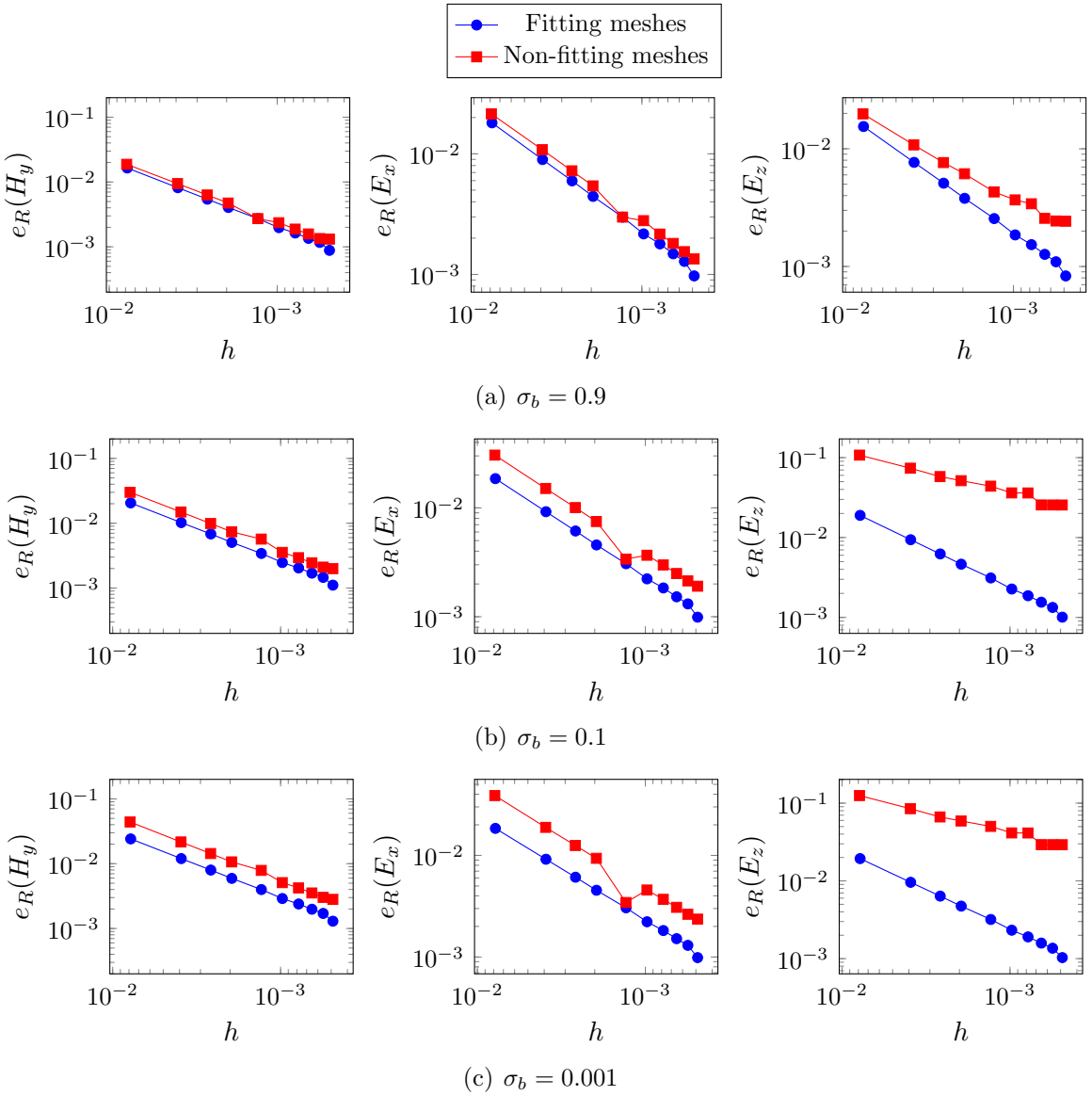

(a) $\sigma_b = 0.9$

(b) $\sigma_b = 0.1$

(c) $\sigma_b = 0.001$

FIGURE 6. Experiment 2

An additional observation is that even for non-fitting meshes, the convergence of $e_R(E_x)$ is linear. Indeed, the non-fitting meshes error is higher than the fitting meshes error only by a constant factor. Such constant increases with the conductivity contrast. While this enhanced accuracy is not proved in our theoretical study, it is not completely surprising, since E_x is the component of the electric field tangential to the interface, and it is therefore continuous across the interface.

3.3.3. *Experiment 3.* In this experiment, we consider a conductivity model with crossing interfaces, generating a singular solution, see subsection 3.2. It is defined by

$$\sigma(x,z) = \begin{cases} 1 & \text{if } x < 0.5, z > 0.5 \\ 0.001 & \text{if } x > 0.5, z > 0.5 \\ 0.1 & \text{if } x < 0.5, z < 0.5 \\ 5 & \text{if } x > 0.5, z < 0.5. \end{cases}$$

As before, since we are in a 2D setting, singularities do not occur in the TE polarization; for this reason, we only consider the TM polarization, and discretize the problem using formulation (28). We keep the same source used in Experiment 2.

As in subsection 3.2, the singularity takes place at the point where the two interfaces cross, namely at point $(0.5, 0.5)$. In order to take into account as much as possible the effect of the singularity in our error measurements, we measure the relative L^2 errors on the set $\tilde{R} = (0.5, 0.7) \times (0.5, 0.7)$. This choice can be physcially interpreted as a receiver located close to the singular point.

Results are presented on Figure 7. At first sight, the curves indicate that the convergence is not of the form $\mathcal{O}(h^s)$ in the asymptotic range. However, this is only because our reference solution is not accurate enough to compute errors correctly, due to the singularity. Nevertheless, we are confident that the convergence rates observed in the pre-asymptotic range are meaningful.

First, we observe that the convergence rates predicted by the error analysis are respected. The magnetic field error decreases as $\mathcal{O}(h^{2s})$ with $s = 1/3$, while the electric field error only behaves as $\mathcal{O}(h^s)$. These observations are valid for both fitting and non-fitting meshes. In particular, this experiment supports our claim that convergence rates are the same for fitting and non-fitting meshes in the presence of a strong singularity.

The accuracy obtained with fitting and non-fitting meshes is equivalent for the electric field. For the magnetic field, the accuracy loss due to the use of non-fitting meshes is a constant factor. In this test-case, fitting meshes are about twice more accurate that non-fitting meshes for the approximation of the magnetic field.

Conclusion

In this work, we have considered the general 3D Maxwell's system with a constant permeability and permittivity and a piecewise constant conductivity. All parameters are scalar valued. We have focused on proving error estimates with optimal convergence rates for first order Nédélec's elements. The main novelty of our analysis is that the convergence rates derived for the electric and magnetic fields are different. If the electric field has regularity H^s, it is well-known that the electric field approximation converges as $\mathcal{O}(h^s)$. Our key result is an improved error estimate for the magnetic field, where we show that the approximation converges as $\mathcal{O}(h^{\min(1,2s)})$. As detailed in Section 2, this result holds for both the E and H-formulation of Maxwell's equations.

We have observed in Section 3 that, in the particular case of a layered medium, our general result implies that the convergence rate for the magnetic field is always linear, regardless of the use of fitting or non-fitting meshes.

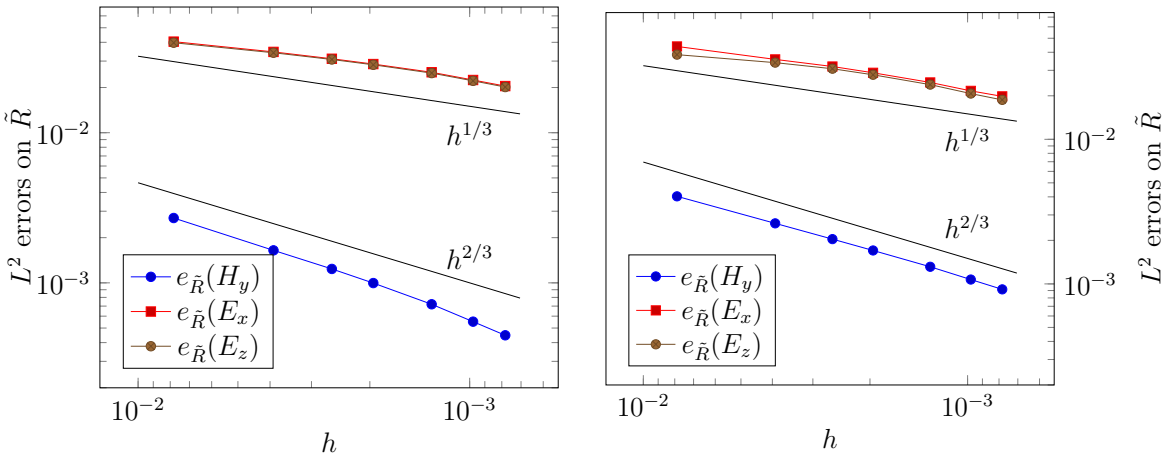

(a) Fitting meshes

(b) Non-fitting meshes

FIGURE 7. Experiment 3

We have illustrated the main features of our convergence analysis using 2D examples, both in TE and TM-polarizations. The predicted convergence rates are observed in all numerical experiments, which makes us confident that our results are optimal. We have also carefully compared fitting and non-fitting meshes. As predicted by the convergence analysis, the results obtained for the magnetic field are similar for both types of meshes. Thus, we advocate the use of non-fitting meshes to approximate the magnetic field without a significant accuracy loss.

In layered media, we have additionally observed that when the conductivity contrast is small, the electric field convergence rate is linear in some preasymptotic range. Also, we have seen that the convergence rate of the component of the electric field tangential to the interface is linear. These two features are not included in our present analysis, and should be the object of future investigations, focused on layered media only.

Although we have considered the 3D Maxwell's system for the proofs, the ideas are rather general and should apply to other systems, such as 2.5D and 2D Maxwell's systems, with minor modifications. Also, the "spirit" of the proof showing that the magnetic field approximation is more accurate might apply to other discretization strategies such as finite difference schemes, and/or numerical methods including averaging techniques.

Future work will be guided towards numerical experimentations on 2.5D and 3D Maxwell's equations in more realistic settings.

ACKNOWLEDGMENTS

David Pardo has received funding from the European Union's Horizon 2020 research and innovation programme under the Marie Sklodowska-Curie grant agreement No 644602, the Projects of the Spanish Ministry of Economy and Competitiveness with reference MTM2013-40824-P and MTM2016-76329-R, the BCAM "Severo Ochoa" accreditation of excellence SEV-2013-0323, and the Basque Government through the BERC 2014-2017

program, the Consolidated Research Group Grant IT649-13 on"Mathematical Modeling, Simulation, and Industrial Applications (M2SI)", and the ICERMAR Project KK-2015/0000097.

Théophile Chaumont-Frelet and David Pardo have received funding from the Projects of the Spanish Ministry of Economy and Competitiveness with reference MTM2016-76329-R.

References

[1] A. Abubakar, T.M. Habashy, V.L. Druskin, L. Knizhnerman, and D. Alumbaugh. 2.5d forward and inverse modeling for interpreting low-frequency electromagnetic measurements. *Geophysics*, 73(4):F165–F177, 2008.

[2] Fournier J. J. Adams R. A. *Sobolev Spaces*. 2nd edition edition, 2003.

[3] D.B. Avdeev. Three-dimensional electromagnetic modelling and inversion from theory to application. *Surveys in Geophysics*, 26:767–799, 2005.

[4] I. Babuška, G. Caloz, and J.E. Osborn. Special finite element methods for a class of second order elliptic problems with rough coefficients. *SIAM J. Numer. Anal.*, 31(4):945–981, 1994.

[5] G.E. Backus. Long-wave anisotropy produced by horizontal layering. *J. Geophys. Res.*, 67:4427–4440, 1962.

[6] H. Barucq, H. Calandra, T. Chaumont-Frelet, and C. Gout. The multiscale medium approximation method in geophysics. *to appear*, 2016.

[7] H. Barucq, T. Chaumont-Frelet, and C. Gout. Stability analysis of heterogeneous Helmholtz problems and finite element solution based on propagation media approximation. *accepted for publication in Mathematics of Computations*, 2016.

[8] A. Bonito, J.L. Guermond, and F. Luddens. Regularity of the Maxwell equations in heterogeneous media and lipschitz domains. *J. Math. Anal. Appl.*, 408:498–512, 2013.

[9] M. Bourlard, M. Dauge, J. M.-S. Lubuma, and S. Nicaise. Coefficients of the singularities for elliptic boundary value problems on domain with conical points III: Finite elements methods on polygonal domains. *SIAM J. Numer. Anal.*, 29:136–155, 1992.

[10] Y. Capdeville, L. Guillot, and J.-J. Marigo. 2-d non-periodic homogenization to upscale elastic media for p-sv waves. *Geophys. J. Int.*, 182:903–922, 2010.

[11] T. Chaumont-Frelet. *Finite element approximation of Helmholtz problems with application to seimsic wave propagation*. PhD thesis, INSA Rouen and Inria EPI MAGIQUE3D, 2015.

[12] T. Chaumont-Frelet. On high order methods for the heterogeneous Helmholtz equation. *accepted for publication in CAMWA*, 2016.

[13] P.G. Ciarlet. *The Finite Element Method for Elliptic Problems*. SIAM, 1978.

[14] S. Constable and L.J. Srnka. An introduction to marine controlled-source electromagnetic methods for hydrocarbon exploration. *Geophysics*, 72(2):WA3–WA12, 2007.

[15] M. Costabel, M. Dauge, and S. Nicaise. Singularities of Maxwell interface problems. *M2AN*, 33(3):627–649, 1999.

[16] F. Dubois. Discrete vector potential representation of a divergence-free vector field in three-dimensional domains: numerical analysis of a model problem. *SIAM J. Numer. Anal.*, 27(5):1103–1141, 1990.

[17] D.V. Ellis and J.M. Singer. *Well logging for earth scientists*. Springer Science & Business Media, 2007.

[18] E. Engström and D. Sjöberg. A comparison of two numerical methods for homogenization of Maxwell's equations. Technical Report TEAT-7121, LUTEDX, 2004.

[19] V. Girault and P.A. Raviart. *Finite Element Methods for Navier-Stokes Equations: Theory and Algorithms (Springer Series in Computational Mathematics)*. Springer-Verlag, 1986.

[20] T.M. Habashy and A. Abubakar. A general framework for constraint minimization for the inversion of electromagnetic measurements. *Progress in Electromagnetic Research*, 46:265–312, 2004.

[21] T.M. Habashy and A. Abubakar. A generalized material averaging formulation for modelling of the electromagnetic fields. *Journal of Electromagnetic Waves and Applications*, 21:1145–1159, 2007.
[22] T.Y. Hou and X.-H. Wu. A mutiscale finite element method for elliptic problems in composite materials and porous media. *Journal of Computational Physics*, 134:169–189, 1997.
[23] P. Ciarlet Jr. On the approximation of electromagnetic fields by edge finite elements. part 1: Sharp interpolation results for low-regularity fields. *Computers and Mathematics with Applications*, 71:85–104, 2016.
[24] J.B. Keller. A theorem on the conductivity of a composite medium. *Journal of Mathematical Physics*, 5:548–549, 1964.
[25] J.L. Lions and E. Magenes. *Non-Homogeneous Boundary Value problems and Applications*. 1972.
[26] P. Monk. A finite element method for approximating the time-harmonic Maxwell equations. *Numer. Math.*, 63:243–261, 1992.
[27] P. Monk. *Finite element methods for Maxwell's equations*. Oxford University Press, 2003.
[28] S. Moskow, V. Druskin, T. Habashy, P. Lee, and S. Davydycheva. A finite difference scheme for elliptic equations with rough coefficients using a cartesian grid nonconforming to interfaces. *SIAM J. NUMER. ANAL.*, 36(2):442–464, 1999.
[29] J.C. Nédélec. Mixed finite elements in R^3. *Numer. Math.*, 35:315–341, 1980.
[30] S. Nicaise. Edge elements on anisotropic meshes and approximation of the Maxwell equations. *SIAM J. NUMER. ANAL.*, 39(3):784–816, 2001.
[31] D. Pardo, L. Demkowicz, C. Torres-Verdin, and M. Paszynski. Two-dimensional high-accuracy simulation of resistivity logging-while-drilling (lwd) measurements using a self-adaptive goal-oriented hp finite element method. *SIAM J. APPL. MATH.*, 66(6):2085–2106, 2006.
[32] D. Pardo, M. Paszynski, C. Torres-Verdin, and L. Demkowicz. Simulation of 3D DC Borehole Resistivity Measurements with a Goal-Oriented hp Finite-Element Method. Part I: Laterogolog and LWD. *Journal of Serbian Society for Computational Mechanics*, 1(1):62–73, 2007.
[33] D. Pardo, C. Torres-Verdin, and L. Demkowicz. Feasibility study for 2d frequency-dependent electromagnetic sensing through casing. *Geophysics*, 72(3):F111–F118, 2007.
[34] C. Sangalli. Capturing small scales in elliptic problems using a residual-free bubbles finite element method. *Multiscale Model. Simul.*, 1(3):485–503, 2003.
[35] J. Schöberl. Commuting quasi-interpolation operators for mixed finite elements. Technical Report ISC-01-10-MATH, Texas A&M University, 2001.
[36] F. Simpson and K. Bahr. *Practical magnetotellurics*. Cambridge University Press, 2005.
[37] M.J. Wilt, D.L. Alumbaught, H.F. Morrison, A. Becker, K.H. Lee, and M. Deszcz-Pan. Crosswell electromagnetic tomography: System design considerations and field results. *Geophysics*, 60(3):871–885, 1995.

T. Chaumont-Frelet, BCAM - Basque Center for Applied Mathematics, Alameda Mazarredo, 14, 48009 Bilbo, Bizkaia
E-mail address: theophile.chaumont_frelet@insa-rouen.fr

S. Nicaise, LAMAV and FR CNRS 2956, Université de Valenciennes et du Hainaut Cambrésis, Le Mont Houy, 59313 Valenciennes Cedex 9, France
E-mail address: snicaise@univ-valenciennes.fr

D. Pardo, UPV/EHU researcher, Ikerbasque Research Professor, BCAM - Basque Center for Applied Mathematics, Alameda Mazarredo, 14, 48009 Bilbo, Bizkaia
E-mail address: dzubiaur@gmail.com